Bioactive Materials 6 (2021) 3580–3595

Contents lists available at ScienceDirect

Bioactive Materials

journal homepage: www.sciencedirect.com/journal/bioactive-materials

A structure-supporting, self-healing, and high permeating hydrogel bioink for establishment of diverse homogeneous tissue-like constructs

Hongqing Chen [a,b,1], Fei Fei [c,1], Xinda Li [d,e,f,g], Zhenguo Nie [h], Dezhi Zhou [d,e], Libiao Liu [d,e], Jing Zhang [i], Haitao Zhang [i], Zhou Fei [a,**], Tao Xu [d,e,j,*]

[a] Department of Neurosurgery, Xijing Hospital, Fourth Military Medical University, Xi'an, 710032, People's Republic of China
[b] Department of Neurosurgery, Central Theater General Hospital, Wuhan, 430010, People's Republic of China
[c] Department of Ophthalmology, Xijing Hospital, Fourth Military Medical University, Xi'an, 710032, People's Republic of China
[d] Biomanufacturing and Rapid Forming Technology Key Laboratory of Beijing, Department of Mechanical Engineering, Tsinghua University, Beijing, 100084, People's Republic of China
[e] Key Laboratory for Advanced Materials Processing Technology, Ministry of Education, Department of Mechanical Engineering, Tsinghua University, Beijing, 100084, People's Republic of China
[f] Department of Neurosurgery, Sichuan Provincial People's Hospital, University of Electronic Science and Technology of China, Chengdu, 610072, China
[g] Chinese Academy of Sciences Sichuan Translational Medicine Research Hospital, Chengdu, 610072, China
[h] Department of Orthopedics, Fourth Medical Center of PLA General Hospital, 100048, Beijing, People's Republic of China
[i] East China Institute of Digital Medical Engineering, Shangrao, 334000, People's Republic of China
[j] Department of Precision Medicine and Healthcare, Tsinghua-Berkeley Shenzhen Institute, Shenzhen, 518055, People's Republic of China

ARTICLE INFO

Keywords:
Time-sharing structure-supporting
High permeability
Bioink
Homogeneous cell growth
Tissue-like constructs

ABSTRACT

The ready-to-use, structure-supporting hydrogel bioink can shorten the time for ink preparation, ensure cell dispersion, and maintain the preset shape/microstructure without additional assistance during printing. Meanwhile, ink with high permeability might facilitate uniform cell growth in biological constructs, which is beneficial to homogeneous tissue repair. Unfortunately, current bioinks are hard to meet these requirements simultaneously in a simple way. Here, based on the fast dynamic crosslinking of aldehyde hyaluronic acid (AHA)/N-carboxymethyl chitosan (CMC) and the slow stable crosslinking of gelatin (GEL)/4-arm poly(ethylene glycol) succinimidyl glutarate (PEG-SG), we present a time-sharing structure-supporting (TSHSP) hydrogel bioink with high permeability, containing 1% AHA, 0.75% CMC, 1% GEL and 0.5% PEG-SG. The TSHSP hydrogel can facilitate printing with proper viscoelastic property and self-healing behavior. By crosslinking with 4% PEG-SG for only 3 min, the integrity of the cell-laden construct can last for 21 days due to the stable internal and external GEL/PEG-SG networks, and cells manifested long-term viability and spreading morphology. Nerve-like, muscle-like, and cartilage-like *in vitro* constructs exhibited homogeneous cell growth and remarkable biological specificities. This work provides not only a convenient and practical bioink for tissue engineering, targeted cell therapy, but also a new direction for hydrogel bioink development.

1. Introduction

Three-dimensional (3D) bioprinting can fabricate biomimetic living tissues, organs, and their functional units *in vitro* through convenient and effective integration of specific cells and biomaterials for a variety of clinical simulation studies [1]. In the most common and affordable microextrusion 3D bioprinting, numbers of hydrogel bioinks have been reported with nontoxicity, biocompatibility, shape retention, and microstructure preservation [1–3]. However, the ready-to-use sol-phase bioinks can cause cell sedimentation, as well as inhomogeneous cell

Peer review under responsibility of KeAi Communications Co., Ltd.

* Corresponding author. Biomanufacturing and Rapid Forming Technology Key Laboratory of Beijing, Department of Mechanical Engineering, Tsinghua University, Beijing, 100084, People's Republic of China.
** Corresponding author. Department of Neurosurgery, Xijing Hospital, Fourth Military Medical University, Xi'an, 710032, People's Republic of China.
E-mail addresses: jujufaces@foxmail.com (H. Chen), feeplus@163.com (F. Fei), feizhou@fmmu.edu.cn (Z. Fei), taoxu@tsinghua.edu.cn (T. Xu).
[1] These authors contributed to this work equally.

https://doi.org/10.1016/j.bioactmat.2021.03.019
Received 3 December 2020; Received in revised form 6 March 2021; Accepted 6 March 2021

distribution in printed constructs [4]. Moreover, extra assistance (low temperature, auxiliary crosslinking, or sacrificial supporting materials) is usually needed to stabilize the structure during printing [5–7]. Among existing bioinks, shear-thinning and/or self-healing gel-phase bioinks are preferred because they are beneficial for maintaining the preset shape during printing while ensuring acceptable cell dispersion [3,8]. These inks, such as nanoengineered kappa-carrageenan, protein-engineered alginate, and β-cyclodextrins/adamantanes functionalized guest-host hyaluronic acid (HA), are mainly dynamically crosslinked [8–10]. Nevertheless, the shape maintenance during printing still relies on temperature control or other assistance since these gel-phase bioinks lack strength for structure-supporting [8–10], while improper temperature control and auxiliary crosslinking are detrimental to cell survival and shape retention [11–13]. Although some structure-supporting hydrogel bioinks reported have overcome the above dilemma, there are some imperfections such as time-consuming preparation process and unsatisfactory printing effect [14,15]. Therefore, it is significant to develop a new ready-to-use and structure-supporting hydrogel bioink.

Printability is a characteristic of hydrogel bioink for microextrusion 3D bioprinting similar to injectability [3,16]. The strength of proper injectable hydrogels based on Schiff base linkages usually spans 3 orders of magnitude [3,17,18], which is sufficient for a variety of structure-supporting options [17,19]. The handiest Schiff base hydrogel is composed of aldehyde hyaluronic acid (AHA) and water-soluble chitosan (such as N-carboxymethyl chitosan, CMC), which owns both biocompatibility and fast gelation capacity (within minutes at room temperature) [17–19]. However, for bioprinted constructs, the structure-supporting property of hydrogels should not only meet the requirements for general shape retention but also microstructure retention. Therefore, how to balance self-healing behavior based on dynamic imide bonds to avoid microstructure fusion is still a challenge (scheme 1A) [20]. Moreover, since Schiff base linkage is easy to hydrolyze in aqueous conditions, most related researches on AHA/CMC system were limited to the fabrication of bulk hydrogels [17–19].

The noncytotoxic succinimidyl active ester functionalized poly (ethylene glycol) (PEG) can react with amino groups of common protein-based materials (such as gelatin, GEL) to form hydrogels through aqueous-stable covalent bonds [21–23], which can make up for the over-fusion of Schiff base hydrogels. For this hydrogel alone, due to the lack of self-healing capacity in stable amide bonds, it could only be lightly crosslinked while used for printing [23]. Meanwhile, it usually takes several hours for this hydrogel to reach the required gelation degree for printing [23], which will reduce the printing efficiency (scheme 1B). Therefore, the fast gelling AHA/CMC hydrogels might make up for this deficiency in return. Additionally, low-permeability hydrogels can cause apoptosis or heterogeneous proliferation of the encapsulated cells due to low matter exchange efficiency (scheme 1E). For the AHA/CMC system, its excellent water absorption and water retention make the hydrogel highly permeable, ensuring the growth of deep cells to facilitate homogeneous tissue repair [17,19].

According to the gelation time difference between the AHA/CMC and GEL/poly(ethylene glycol) succinimidyl glutarate (PEG-SG) hydrogels, we propose a time-sharing (TSH) strategy and present a time-sharing structure-supporting (TSHSP) ink formulation through simple mixing. The fast gelling AHA/CMC hydrogel can make the bioink ready-to-use, and a slow continuous gelling system, GEL/PEG-SG used in our study can maintain the construct stability during printing (scheme 1C). We optimized the formulation and verified the crosslinking effect of each gelation system in this composite hydrogel, which possessed balanced viscoelastic behavior, self-healing behavior, and high permeability. Then we tested the printability of the hydrogel and the aqueous durability of printed constructs. Cell viability and proliferation in printed constructs were evaluated during 21 days of culture. Nerve-like, muscle-like, and cartilage-like *in vitro* constructs were successfully printed where different cells manifested a homogeneous growth, as well as the biological specificities (scheme 1D). We envision that this TSHSP bioink with high permeability can provide a convenient and practical solution not only for tissue engineering but also for targeted cell therapy.

2. Experimental section

2.1. Oxidation of HA

AHA was obtained by oxidating HA (Mn = 1000–1500 kDa, 1604073, Freda, China) with sodium periodate. In brief, 1% (w/v%) aqueous HA solutions in ultrapure water were prepared at 60 °C and cooled down to room temperature. According to different theoretical oxidation percentages, the corresponding volume of 0.5 M sodium

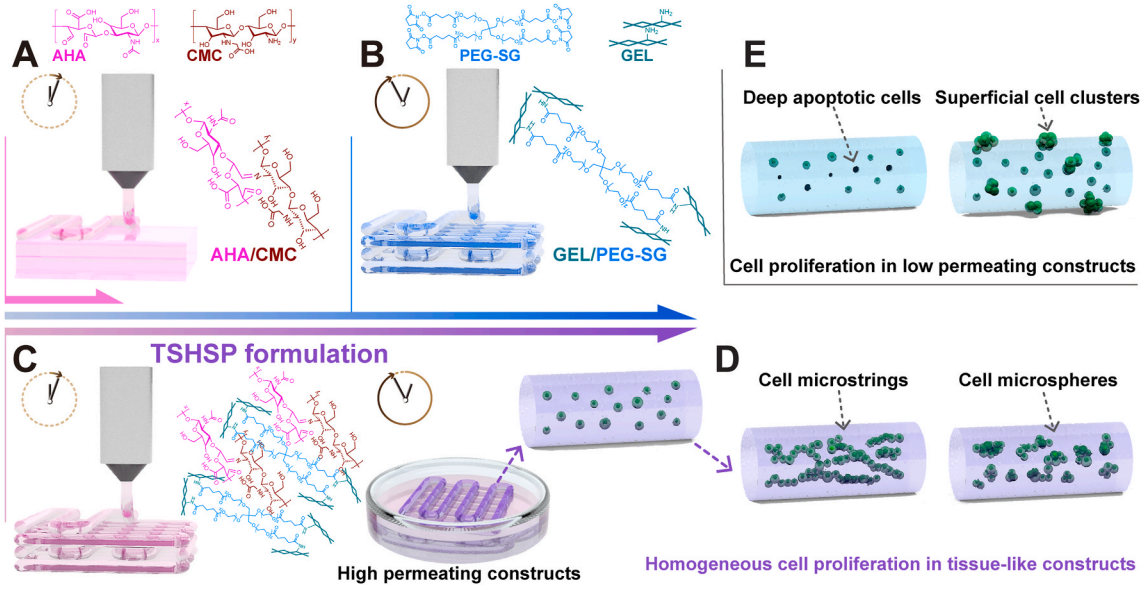

Scheme 1. (A) Microstructure fusion of constructs printed with fast gelling AHA/CMC hydrogel due to dynamic covalent imine bonds. (B) Time-consuming pre-printing preparation of slow gelling GEL/PEG-SG hydrogel based on stable covalent amide bonds. (C) The TSHSP hydrogel realized by the complementarity of AHA/CMC and GEL/PEG-SG. (D) The uniform proliferation pattern of cells in tissue-like constructs printed with TSHSP formulation varies with cell types. (E) The proliferation pattern of cells in low permeating constructs.

periodate aqueous solutions were used to react with HA in the dark for 24 h. Ethylene glycol with a volume of 1/10 of the added sodium periodate solutions was used to inactivate the residual sodium periodate for 2 h. Then the solutions were dialyzed (MD34, MWCO 14000) against ultrapure water for 3 days at room temperature with the water refreshed every 8 h. Solid AHA was obtained by lyophilizing the solutions and stored at 4 °C.

2.2. Aldehyde assay

The oxidization percentage of AHA was quantified by measuring the content of aldehyde groups with *tert*-butyl carbazate (*t*-BC). Similar to the manner of hydrazone formation, carbazates can react with aldehydes to form stable carbozones [24]. After excess carbazates reacted with AHA, excess aqueous 2,4,6-trinitrobenzene sulfonic acid (TNBS) solutions were added to form a colored complex (trinitrophenyl derivative) with the residual carbazates, the absorbance of the colored complex was then measured to determine the residual carbazates. The carbazates consumed by AHA was calculated from the residual carbazates and then used to quantify the aldehyde content in the sample. Briefly, equal volumes of 5% (w/v%) aqueous AHA solutions and 30 mM t-BC solutions in 1% trichloroacetic acid were mixed and reacted at room temperature for 24 h. Then the mixture and 6 mM TNBS solutions in 0.1 mM borate buffer (pH 8.0) were mixed at a volume ratio of 1:10 and reacted for 1 h. The colored complex formed by the reaction was then diluted 2 times by 0.5 M aqueous hydrochloric acid, and the absorbance was measured at 334 nm (Epoch 2, Biotek). The blank was prepared by mixing trichloroacetic acid without *t*-BC and the remaining components in the same manner. Gradient concentrations of aqueous *t*-BC solutions were used as standards to obtain a calibration curve for quantifying the residual carbazates. The oxidation percentages of AHA were calculated based on the number of glucuronates.

2.3. Bioink preparation

All stock solutions of different concentrations (w/v%) were prepared with phosphate buffer saline (PBS) (Gibco). Four-arm PEG-SG (Mn = 10000, 06020702909, SINOPEG, China) solutions were prepared just before use. Other solutions were prepared in advance and stored at 4 °C. In brief, the AHA stock solutions (3%, 4%, and 5%) were prepared at 4 °C overnight. The PEG-SG stock solutions (0.5%, 1%, 2% and 3%) were prepared at room temperature. CMC (Mn = 100000-200000, carboxylation degree: 83.42%, C832672, MACKLIN, China) stock solutions (2%, 3%, 4%, and 5%) and GEL stock solutions (3%, 4%, and 5%) were prepared at 37 °C. Both AHA and PEG-SG stock solutions were sterilized by filtration at 0.22 μm. The CMC and GEL stock solutions were pasteurized for sterilization (maintain at 70 °C and 4 °C for 30 min respectively as a cycle, 3 cycles in total). The optimal concentration of each solution was determined by rheological testing. The bioink was prepared by mixing each solution in equal volumes (1:1:1:1) at room temperature as follows: CMC and GEL stock solutions were mixed to prepare the CMC-GEL solutions, AHA and PEG solutions were mixed to prepare the AHA-PEG-SG solutions to resuspend cells, the CMC-GEL solutions and the cell-containing AHA-PEG-SG solutions were finally mixed with two syringes to form the AHA/CMC-GEL/PEG-SG hydrogel bioink, which is the TSHSP bioink.

2.4. Rheological analysis

A Haake RheoStress 1 rheometer (Thermo science, Germany) with a cone-plate fixture (C35/2°Ti L) was used for rheological examination to characterize the gelation time, mechanical properties, and recovery behavior of hydrogels. The gap size was 1 mm and the temperature during the test was 25 °C. The stock solutions returned to room temperature were loaded onto the plate and mixed with a pipette for 3 s. To test the gelation time, an oscillation time sweep (CS, 3 Pa, 0.5 Hz) was performed to observe the changes of the storage (G′) and loss modulus (G″) over time. Then an oscillation frequency sweep (CD-AS, 0.01–1 Hz, 1% strain) or an oscillation amplitude sweep (CD-AS, 0.1%–10000% strain, 0.5 Hz) was followed to show the frequency dependence of G′ and G″, and failure strain of hydrogels, separately. To test the instantaneous recovery ability of hydrogels, a 5-cycle deformation test was performed in the form of oscillation time sweeps under alternating strain (CD-AS, 800% and 1% strain, 0.5 Hz, 200 s per cycle) after 30 min of the initial gelation time test.

2.5. Macroscopic gelation

Each stock solution was transferred into a 5 mL centrifuge tube and the tubes were vibrated for 5 s and left for 15 min. Then the tubes were inverted to observe whether the ink exhibited a gel-phase. Every one or two stock solutions were excluded to clarify which components were mainly involved in sol-gel transition at a given concentration. If the mixture flowed down the wall of the tube, it was considered to be a sol-phase even if a crosslinking did occur, since this was not enough to make hydrogel structure-supporting.

2.6. Fourier-transform infrared spectroscopy (FT-IR) measurements

To perform the FT-IR analysis, all solutions were prepared with ultrapure water. Hydrogels were formulated and lyophilized. The FT-IR spectra of lyophilized AHA/CMC, GEL/PEG-SG, and the TSHSP hydrogels were measured in the range of 4000–400 cm^{-1} using a PLATINUM Diamond ATR accessory VERTEX 70 spectrometer (Bruker Daltonics, Germany). Moreover, the spectra of HA, AHA, CMC, PEG-SG, and GEL were also measured.

2.7. Macroscopic self-healing and permeating assay

In addition to rheological deformation-recovery tests in the manner of oscillation time sweeps under alternating strain as described above, the macroscopic self-healing properties of TSHSP hydrogels were also observed. The AHA-PEG-SG solutions dyed with red or blue food dyes were mixed with the CMC-GEL solutions and left for 10 min. The formed hydrogels were cut into small pieces with a size of 5 mm × 5 mm × 5 mm. Small pieces of different colors were placed next to each other without any external stimulus. The healing effect was confirmed by lifting the hydrogel to see if it can bear its own weight without falling apart. For the macroscopic permeating test, the healed hydrogel was sealed and kept at 37 °C until the color of the entire hydrogel became uniform. Then the uniformly colored hydrogels were immersed into PBS and kept at 37 °C to allow the food dyes to permeate out. At last, the yellow food dyes were added into PBS to observe its permeation back into hydrogels. The permeating time was recorded, respectively.

2.8. 3D printing of hydrogels

Formulated TSHSP hydrogel was prepared by mixing CMC-GEL and AHA-PEG-SG solutions with two syringes for 20 s. Then the hydrogel-filled syringe was fitted with a 25G (ϕ = 0.26 mm) nozzle and loaded into a bioprinter (Livprint Norm, Medprin, China). The printing parameters were set as follows: 90° interlayer offset, 30% infill rate, 6 mm/s linear speed, 0.07 mL/min extrusion speed, and the temperature control off. The 6-layer printed structures were immersed in freshly prepared 4% (w/v%) PEG-SG solutions for 3 min and washed 3 times with PBS. The AHA/CMC and 5% GEL-1% alginate (ALG, w/v%, final concentrations) hydrogels were used for printing as controls. The printing parameters of AHA/CMC were the same as TSHSP, and the parameters of GEL-ALG were also the same as TSHSP except that the printing temperature was set to 10 °C.

2.9. Durability testing of printed constructs

After washing with PBS, the printed constructs were transferred in high glucose Dulbecco's Modified Eagle Medium with L-glutamine and pyruvate (HG-DMEM, 11995065, Gibco) containing 10% fetal bovine serum (FBS, 10099141, Gibco), 100U/mL penicillin, and 100 μg/mL streptomycin (15140122, Gibco), and incubated at 37 °C and 5% CO2 to evaluate their structural durability and stability in cell culture conditions. As controls, AHA, CMC, GEL, and PEG-SG solutions were mixed in a volume ratio of 2:2:1:1 and 1:1:2:2 to print the constructs, respectively.

2.10. Cell culture

In this work, four types of cells were used. NIH/3T3 fibroblasts (CRL1658) and C2C12 myoblasts (CRL1772) from ATCC™ were kindly provided by the Cell Bank, Chinese Academy of Sciences (Kunming, China). The NE-4C neural stem cells (CRL-2925, ATCC™) was kindly provided by the Stem Cell Bank, Chinese Academy of Sciences (Shanghai, China). Cells were cultured at 37 °C and 5% CO_2. NIH/3T3 and C2C12 cells were cultured in HG-DMEM containing 10% FBS, 100U/mL penicillin, and 100 μg/mL streptomycin. NE-4C cells were cultured in Minimum Essential Medium (MEM, 11090081) supplemented with 10% FBS, 1% GlutaMAX™ (35050) and 1% Non-Essential Acids (11140), which were all from Gibco. Articular chondrocytes were isolated from the knee joints of New Zealand white rabbits aged 2 weeks (from Animal Center of East China Institute of Digital Medical Engineering, Shangrao, China). In brief, After the rabbits were sacrificed, the articular cartilage was harvested and washed 3 times with PBS. Then, the articular cartilage was cut into 1×1 mm^2 pieces and predigested by 0.25% trypsin (25200056, Gibco) at 37 °C and 5% CO_2 for 30 min. After washed with PBS, cartilage pieces were digested by 0.2% collagenase type II (17101015, Gibco) at 37 °C and 5% CO_2 overnight. The digested solutions were centrifuged at 1500 rpm for 10 min, and the harvested cells were washed twice with PBS. The cells were cultured at a density of $4 \times 10^4/cm^2$ in HG-DMEM containing 10% FBS, 100U/mL penicillin, 100 μg/mL streptomycin, and 1% L-Ascorbic acid 2-phosphate (49752, Sigma). The chondrocytes were cultured to passage 3 with medium refreshed every 48 h.

2.11. 3D bioprinting and culture of cell-laden constructs

Cell-containing AHA-PEG-SG solutions and CMC-GEL solutions were gently mixed with two syringes for 20 s. 6-Layer grid structures were printed out with a size of 12 × 12 mm at room temperature and crosslinked with 4% PEG-SG solutions for 3 min. Then the cell-laden constructs were transferred into 6 well ultra-low attachment plates (Corning 3473, USA) and cultured at 37 °C and 5% CO2 after rinsed 3 times with PBS. For 5%GEL-1%ALG bioinks, an equal volume of cell suspension and pre-warmed 10%GEL-2%ALG stock solutions were mixed, and the constructs were then printed at 10 °C and crosslinked with 3% sterilized calcium chloride solutions for 3 min. The final concentration of NIH/3T3, NE-4C, C2C12, and Chondrocytes in bioink was 1.5×10^6/mL, 1×10^7/mL, 9×10^6/mL, and 2×10^7/mL, respectively.

2.12. Live/dead assay

Cell viability in constructs was evaluated by the cellular imaging and flow cytometry using the Live/Dead viability/cytotoxicity assay kit (KGAF001, KeyGEN BioTECH, Nanjing, China) according to the manufacturer's instructions. Briefly, cell-laden TSHSP hydrogel constructs were stained with freshly prepared 2 μM calcein-AM and 8 μM propidium iodide (PI) solutions at room temperature for 30 min. After images were taken by an inverted fluorescence microscope (Nikon Eclipse Ti2-u, Japan), the constructs were hydrolyzed by 0.25% trypsin at 37 °C for 3min and separated by a pipette for 30 s. Medium with 10% FBS was used to react with the residual trypsin. The proportions of different color-stained cells were analyzed using a flow cytometer (CytoFLEX, Beckman Coulter Life Sciences) after diluted with PBS. GEL-ALG constructs were dissolved by 55 mM sodium citrate and 20 mM ethylenediamine tetraacetic acid solutions (also used in TSHSP hydrogel constructs to ensure the consistency of cell processing) in normal saline and 0.25% trypsin to isolate cells. Each type of cell-free construct was used to help define the cell ranges and analyze backgrounds. Cells cultured in 2D were used as negative controls, while those cultured with 0.1% (v/v%) apoptosis inducers A and B of an Apoptosis Inducers Kit (C0005, Beyotime, Shanghai, China) for 24 h were positive controls.

2.13. Cell proliferation assay

Cell proliferation assay was performed with the Alamar Blue Kit (40202ES76, YEASEN, Shanghai, China). In brief, NIH/3T3 constructs (2.5×10^6 cells) were cultured with 3 mL of fresh 10% (v/v%) Alamar Blue solutions in HG-DMEM for 2 h. The absorbance of reacted solutions was measured at wavelengths of 570 nm and 600 nm. Then the cell-laden constructs were continued to be cultured in fresh medium. The DNA replication rate of cells was detected by flow cytometry using the Cell-Light ethynyl-deoxyuridine (EdU) DNA Cell Proliferation kit (containing EdU, Apollo staining buffer, and Hoechst 33342; C10338-3, Ribobio, China). Briefly, cell-laden constructs were cultured with fresh 20 μM EdU solutions for 12 h. Then, the EdU-labeled cells in constructs were incubated with Apollo fluorescent staining buffer for 30 min and stained with Hoechst 33342 for 30 min after washed twice with PBS. After the constructs were washed, dissolved, and diluted as described above, the distribution of cells with different proliferation performance was analyzed by the flow cytometer. The cell-free constructs and cell-laden constructs without EdU labeling (negative controls) were used to help define the cell-range and analyze the background of dyes, respectively. Proliferation analyses of GEL-ALG constructs were also performed in the same manner.

2.14. Fabrication of tissue-like constructs

As described above, NE-4C, C2C12, and chondrocyte bioinks were prepared and used to print the *in vitro* tissue-like models in the form of a 12 × 12 cm, 6-layer grid structure at room temperature, respectively. After 7 days of adaptive culture with MEM, the NE-4C constructs were treated with 10^{-6} M all-trans retinoic acid (ATRA) (T1850000, Sigma-Aldrich) for 7 days to perform neural differentiation, and then cultured for another 7 days without ATRA. C2C12 constructs were cultured in HG-DMEM for 7 days and then in DMEM/F-12 (11210033, Gibco) with 1% horse serum (26050070, Gibco) for 14 days to induce muscle cell differentiation. Articular chondrocyte constructs were cultured with HD-DMEM containing 1% L-Ascorbic acid 2-phosphate for 21 days. All types of medium were refreshed every 48 h.

2.15. Immunohistological analyses

After 21 days of culture, the constructs were fixed with 4% paraformaldehyde at 4 °C overnight, and then subjected to gradient dehydration with sucrose solutions (10%, 20%, 30%). After absorbing moisture with filter paper and embedding with OCT, samples were cut into 5 μm thick sections after being trimmed to the maximum diameter along the longitudinal axis of microfilament.

For the NE-4C constructs, immunofluorescence staining of nestin and β III-tubulin were performed. In nestin staining, the sections were incubated with a blocking buffer for 60 min and then incubated with anti-nestin primary antibody (1:100, ab11306, Abcam) at 4 °C overnight. Next, the sections were incubated with Alexa Fluor 488-labeled secondary antibody (A0428, Beyotime) for 1 h at room temperature. In βIII-tubulin staining, the sections were incubated with anti-βIII tubulin primary antibody (1:500, ab18207, Abcam) and Alexa Fluor

555-labeled secondary antibody (A0453, Beyotime) in sequence. The cell nuclei were stained with DAPI for 10 min. For C2C12 constructs, in desmin immunofluorescence staining, the sections were incubated with anti-desmin primary antibody (1:500, ab15200, Abcam) and Alexa Fluor 488-labeled secondary antibody. In myosin immunofluorescence staining, anti-fast myosin skeletal heavy chain primary antibody (1:250, ab91506, Abcam) and Alexa Fluor 555-labeled secondary antibody was used. For chondrocyte constructs, In immunofluorescence staining of collagen type II, the sections were incubated with anti-collagen II primary antibody (1:50, ab185430, Abcam) and Alexa Fluor 488-labeled secondary antibody in sequence. In all negative controls, PBS was used instead of the primary antibody. Sulfated glycosaminoglycans (sGAG) were stained with Alcian Blue (pH 1.0, G1563, Solarbio) for 20 min.

Images were captured with a fluorescence microscope (Nikon Eclipse SCi-S, Japan) while ensuring the same exposure time of the same type of markers. The semi-quantitative analyses were performed using ImageJ. For immunofluorescence staining, a threshold was set to distinguish the staining from the background properly, and then the original mean pixel intensity (MPI) per field was measured. The MPI of negative controls was also measured in the same way, which was subtracted from the original MPI to exclude non-specific staining. For alcian blue staining, the positive area ratio (% area) was measured. The final cell density was also achieved using Image J. After the threshold was set, the % area of DAPI staining within the range of the printed filaments was analyzed at 10 random locations. The coefficient of variation (CoV, SD/mean) of % area of DAPI was used to evaluate the dispersion degree of cells/cell clusters distribution.

2.16. Statistical analysis

The results are expressed as mean ± SD. Two-tailed Student's t-tests were used to analyze the statistical difference between two sets of data with equal variances. Welch's corrections were applied when the variances were uneven. F-tests were used to compare the variances. $P < 0.05$ was considered statistically significant.

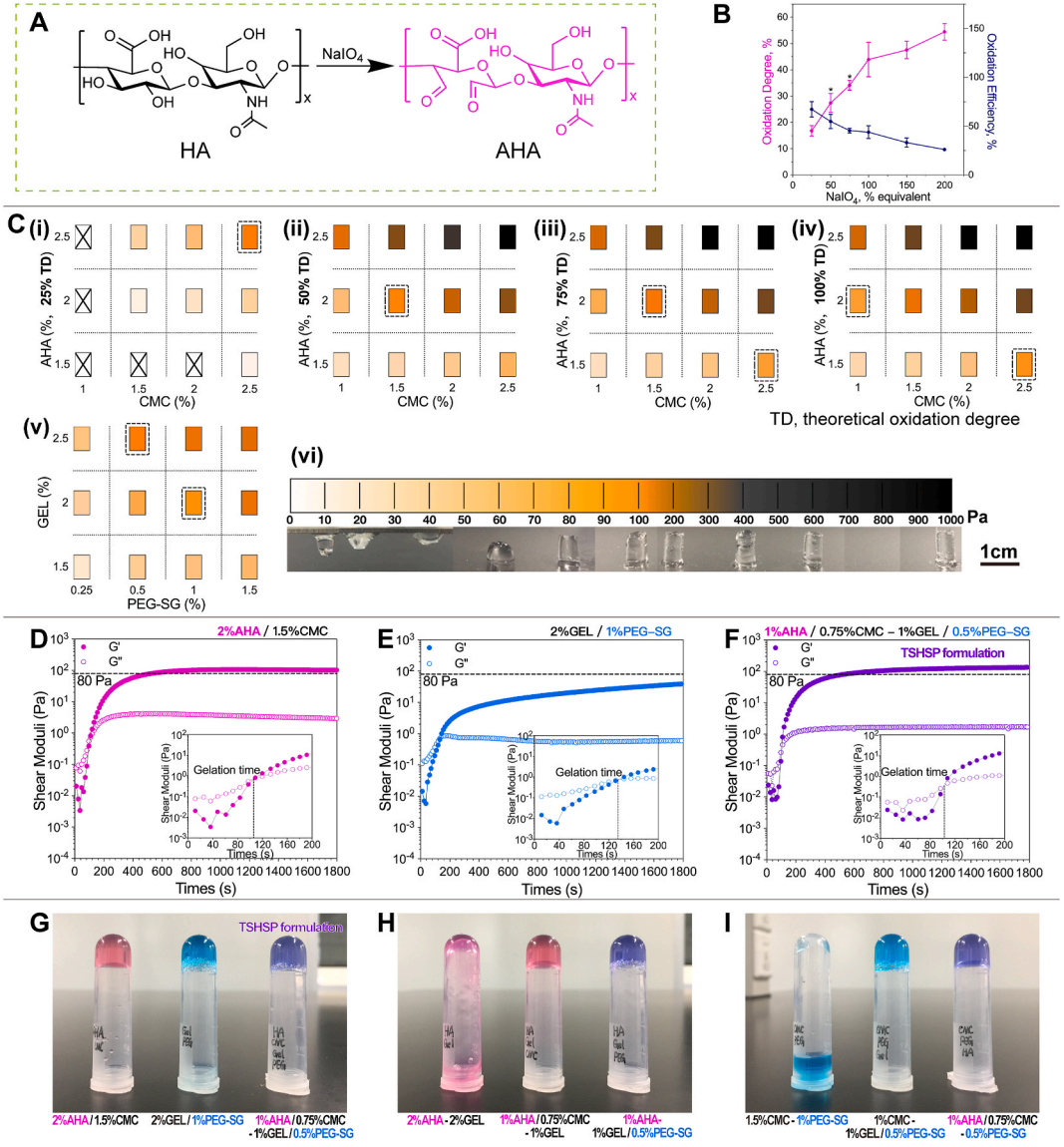

Fig. 1. Optimization of TSHSP hydrogel formulation. (A) Schematic diagram of HA oxidation. (B) Actual oxidation degree and oxidation efficiency profile of AHA under different sodium periodate equivalents (n = 3, error bars, mean ± SD). (C) G'_{max} distribution of AHA/CMC (i-iv) and GEL/PEG-SG (v) hydrogels under different formulations, macroscopic appearance of AHA/CMC hydrogels with different G'_{max} (vi). (D)–(F) Gelation profile of AHA/CMC (D), GEL/PEG-SG (E), and TSHSP (AHA/CMC-GEL/PEG-SG, F) formulation. (G)–(I) Macroscopic appearance of AHA/CMC, GEL/PEG-SG, TSHSP formulations (G), AHA-GEL mixture (H), and CMC-PEG-SG mixture (I). $^*P < 0.05$, over previous oxidation degree.

3. Results

3.1. Optimization of TSHSP hydrogel formulation

While HA is oxidized by sodium periodate, the C–C bond of cis vicinal diols in D-glucuronic acid is cleaved to generate the dialdehyde derivative, AHA (Fig. 1A) [25]. Through the aldehyde assay, we used the reacted carbazates to determine the content of aldehyde groups in AHA. Then the actual oxidation degrees were calculated according to the percentages of aldehydes in gluconates. The oxidation efficiency was calculated based on the actual and theoretical oxidation degree. With the increase of sodium periodate, the oxidation degree of AHA rose accordingly, while the oxidation efficiency decreased (Fig. 1B).

In this study, we used AHA with theoretical oxidation degrees of 25%, 50%, 75%, 150%, and 200% were used to react with CMC, respectively. Gelation was realized through the Schiff base reaction between the amino groups of CMC and the aldehyde groups of AHA [26]. The maximum G' (G'_{max}) of AHA/CMC formulations during crosslinking ranged ~ 8–950 Pa (Fig. 1C(i - v) and figure S1). The G'_{max} of AHA/CMC appeared within 30min, and its value was positively associated with the oxidation degree and the concentration of each component (Fig. 1C(i - v) and Fig. S1; Table 1, Table S1). To observe the relationship between the G′ and shape retention of hydrogels macroscopically, we used 1 mL syringes with the distal ends removed as molds, added 0.2 mL of different AHA/CMC formulations according to the specific G'_{max} measured by the rheometer, and took out the hydrogels after 30 min. The hydrogel was structure-supporting when the G'_{max} was ~80 Pa and didn't show significant deformation when G'_{max} reached 200 Pa (Fig. 1C(vi)). Since stiffer hydrogels will cause more damage to cells during deformation, we preferred hydrogel formulations with G'_{max} close to 80 Pa. Considering the practicality of AHA's oxidation degree/efficiency, proper concentration of components, appropriate gelation time, the reaching time of 80 Pa G' (Time $_{80Pa}$) that facilitates printing, we selected the hydrogel containing 2% AHA (theoretical oxidation degree, 50%; actual oxidation degree, 27.45 ± 3.60%; oxidation efficiency, 54.90 ± 7.21%) and 1.5% CMC (Fig. 1C(ii)). In AHA/CMC formulation, the sol-gel transition occurred at ~110 s and the hydrogel became structure-supporting at ~9 min (Fig. 1D, Table 1). For GEL/PEG-SG hydrogels, the crosslinking between primary amine groups of GEL and succinimidyl esters occurred slower, and G′ didn't reach the maximum even at 1 h (Fig. S3), indicating a slow continuous gelling property compared with AHA/CMC system. Here we used the G′ at 1 h (G'_{1h}) to determine appropriate structure-supporting hydrogels. The hydrogel containing 2% GEL and 1% PEG-SG were selected (Fig. 1, C(v) and E, Table 1). We obtained the TSHSP hydrogels by mixing the above two hydrogel formulations in equal volumes (AHA/CMC-GEL/PEG-SG, mass ratio, 4:3:4:2; volume ratio, 1:1:1:1; concentrations, 1% AHA, 0.75% CMC, 1% GEL, 0.5% PEG-SG) with a limited increase of G'_{max} (Fig. 1F and G, Table 1). The rheological characteristics were similar to that of AHA/CMC hydrogels in the early stage (fast time phase) and similar to that of GEL/PEG-SG hydrogels in the later stage (slow time phase) during gelation (Fig. 1, D-F). Theoretically, this allows the hydrogel to be printed within a short time after preparation and maintain structural stability during printing.

The macroscopic gelation of TSHSP hydrogel was consistent with the rheological results (Fig. 1G). The mixture containing 2%AHA-2%GEL did not show a gel-phase, which was also confirmed by rheological analysis (Fig. S4). The macroscopic gelation occurred after adding the stock solutions of CMC or PEG alone according to the ratio of the TSHSP formulation (the missing ingredients were replaced by an equal volume of PBS, Fig. 1H). The test for 1.5%CMC-1%PEG-SG mixture showed the same results (Figs. 1I, S4). This indicates that the AHA/CMC and GEL/PEG-SG systems were mainly responsible for gelation in TSHSP hydrogel formulation.

Table 1
Rheological data of TSHSP hydrogel formulation (n = 3, mean ± SD).

	Time $_{G'=G''}$ (s)	Time $_{80Pa}$ (s)	Time $_{G'max}$ (s)	G'_{max} (Pa)	G'_{30min} (Pa)
2%AHA (50% TD)/1.5% CMC	109.78 ± 9.86	544.57 ± 66.06	799.91 ± 154.20	96.86 ± 12.73	94.67 ± 10.75
2%GEL/1% PEG	136.13 ± 7.21	3016.40 ± 388.25	>1 h	88.32 ± 5.32[a]	39.94 ± 2.18
TSHSP formulation	99.83 ± 14.28	500.36 ± 29.79	>30min	133.13 ± 5.13[b]	133.13 ± 5.13

[a] $G'_{max} = G'_{1h}$.
[b] $G'_{max} = G'_{30min}$.

3.2. Chemical characterization

The infrared spectra were shown in Fig. 2. For AHA, we monitored the symmetric vibrational band (carbonyl) around 1730 cm^{-1} [24] and out-of-plane vibrational band (C–H) around 836 cm^{-1} [27] in aldehyde groups. For CMC, the band corresponding to carboxy and carboxymethyl groups were monitored around 1580 and 1403 cm^{-1} [28,29], respectively. For the AHA/CMC hydrogels, with the chemical crosslinking of aldehyde and amino functions via Schiff-base linkages, the vibrational band of the hemiacetal structures appeared at 889 cm^{-1} with the disappearance of aldehyde-based bands [17]. The band of imine groups (N═C, around 1650 cm^{-1}) was not shown separately, which should be overlapped with the band of the carboxy groups [30]. For GEL/PEG-SG hydrogels, the imide groups band (1640 cm^{-1}) [31], the carbonyl bands of esters and five-membered imide rings (1800-1700 cm^{-1}) [32,33] in PEG-SG disappeared when the succinimidyl esters reacted with the primary amine of GEL. The carbonyl bands of crosslinked amide I in hydrogels coincided with the amide I band of GEL (1632 cm^{-1}) [34]. The bands of amide II and III (1537 and 1235 cm^{-1}) [34] were also not altered, while the transmittance of characteristic bands (CH2, 2870 and 1460 cm^{-1}; C–O–C, 1089 cm^{-1}; crystallization, 960 and 840 cm^{-1}) [35] of PEG increased due to the decrease in the concentrations of these groups that did not undergo crosslinking. The infrared spectrum of TSHSP hydrogel was similar to that of the AHA/CMC and GEL/PEG-SG hydrogels. There was a broad band in the range of 1700–1490 cm^{-1}, which could be formed by overlapping the bands of carboxy groups in CMC and AHA, imine groups in AHA/CMC hydrogel, amide I in GEL/PEG-SG hydrogel, amide I and II in GEL.

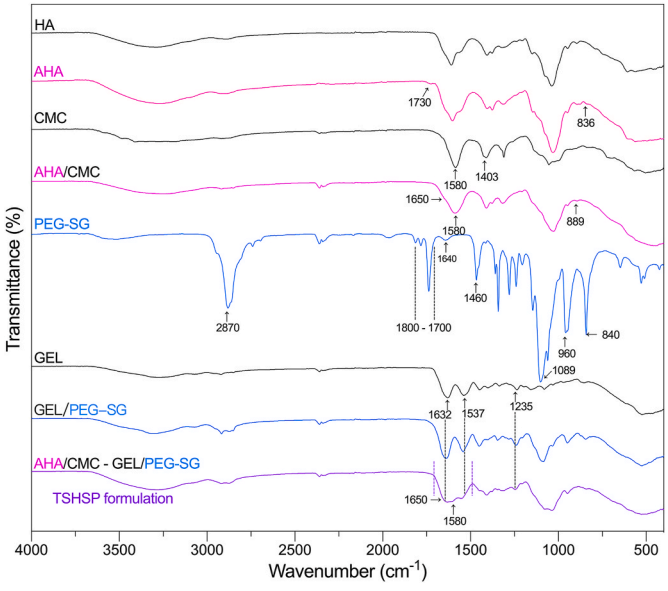

Fig. 2. FT-IR spectra of HA, AHA, CMC, PEG-SG, GEL, and the AHA/CMC, GEL/PEG-SG, TSHSP hydrogels.

3.3. Viscoelastic behavior

After a 30 min-oscillation time sweep for the gelation test, we performed the oscillation frequency sweep. The G′ was almost independent of frequency and remained over the G″ in the linear viscoelastic region, indicating that all three mixtures achieved stable gelation (Fig. 3A). The G′ of TSHSP hydrogel increased due to the reinforcement of the dual crosslinked interpenetrating network of AHA/CMC and GEL/PEG-SG (Fig. 3A). Since the slow-gelation of GEL/PEG-SG continued after 30 min, the G′ of TSHSP hydrogels also showed a gently rising trend similarly (Fig. 3A). The shear-thinning characteristic enables hydrogel bioinks to be printed through the nozzle without breaking [9]. Under oscillatory measurements, the complex viscosity (|η*|) of all samples decreased with increasing frequency (Fig. 3B), showing clear shear-thinning behavior [36,37], indicating that the formulation had the potential to perform printing (Fig. 3B). For the viscosity that can increase with the degree of cross-linking [38], the TSHSP hydrogel showed a higher |η*| (Fig. 3B), which can ensure better flow performance and faster shape recovery during printing [1,39]. As the value of G''/G′, the loss tangent (tan δ) can reflect the elastic response at low frequency for cross-linked hydrogel [40]. The tan δ of all samples was <1 and decreased with the increase of frequency, showing more elastic behavior (Fig. 3C). In microextrusion bioprinting, a higher tan δ can benefit extrusion uniformity, while a lower tan δ can benefit structural integrity [41]. Here, we found that the tanδ of TSHSP hydrogel is between that of AHA/CMC and GEL/PEG-SG hydrogel (Fig. 3C), which can meet the above two requirements of printing in a more balanced manner in terms of rheology.

3.4. Self-healing performance and permeability

3.4.1. Self-healing behavior

Covalently cross-linked hydrogels might suffer strain-induced network damage during extrusion printing. The self-healing hydrogel can not only prevent printing filament from breaking, but also ensure structural integrity and shape retention. Before the cyclic deformation test, we performed the oscillation amplitude sweep to find the yield strain at which the hydrogel becomes fluid-like. The strain was about 300%, 600%, and 600% when G'' > G′ in AHA/CMC, GEL/PEG-SG, and TSHSP hydrogels, respectively. These results indicates that the stable GEL/PEG-SG network is dominant in the yield strain of the overall TSHSP hydrogels (Fig. 4A–C). Then we applied 800% and 1% strain for the cyclic deformation test. We noticed that both AHA/CMC and GEL/PEG-SG could not entirely recover after deformation (Fig. 4D and E). The G′ of AHA/CMC hydrogel gradually decreased after each deformation cycle (Fig. 4D). This was related to the instability of the reversible Schiff base linkages in the presence of water, which can tilt the equilibrium towards the starting materials [42]. With the continuous slow phase crosslinking between GEL and PEG-SG (Fig. S3), the G′ of the hydrogel gradually increased after the second deformation (Fig. 4E). Therefore, the complementary of these two deformation-recovery characteristics enabled TSHSP hydrogel to recover entirely after deformation (Fig. 4F). We also observed the macroscopic self-healing behavior of TSHSP hydrogel. After putting the separated hydrogel blocks stained with different food dyes next to each other without any external stimuli for 10 min at room temperature, obvious fusion occurred at the contact interface (Fig. 4G(i)). The healed hydrogels were able to bear their own weights, and no separation occurred at the fusion interfaces (Fig. 4G(ii, iii)).

3.4.2. Hydrogel permeability

We evaluated the permeability of TSHSP hydrogel macroscopically in an intuitive way. The healed hydrogel with uniform color was immersed in PBS and kept at 37 °C. The food dyes escaped a lot from the hydrogel after 20 min and almost totally infiltrated into the PBS after 2 h (Fig. 4H(i)). While other food dyes were added into PBS, they could also infiltrate into the hydrogel effectively after 2 h (Fig. 4H(ii)). This high-grade permeability might provide a reliable foundation for matter exchange.

3.5. Properties of cell-free constructs

3.5.1. Printability of hydrogels

For verifying the rheological properties, hydrogels were printed as common grid constructs at room temperature. After the formulation was mixed for only 20 s, the TSHSP hydrogel could be extruded from the printer nozzle (25G, $\phi = 0.26$ mm) into continuous filaments with a diameter of 0.46 ± 0.053 mm (Fig. 5A and Fig. S2). Including the preparation time of the printer, it took about 3 min from ink mixing to printing, which is still much shorter than the 500 s required for G′ to reach 80Pa in the rheological tests (Table 1). This is because the formulation was mixed more thoroughly in printing than in the rheological tests and ink crosslinking was accelerated. Moreover, integrated structure-supporting constructs were obtained in multiple-sample printing and larger sample printing (Fig. 5B, Fig. S5). It was the fast crosslinking of AHA/CMC that ensured immediate printing after the formulation was prepared, while the slow phase crosslinking of GEL/PEG-SG helped achieve structural stability during printing (Fig. 5C(i)). We also left the TSHSP formulation for an additional 30 min after 20 s of mixing and got the same printing effect. For GEL/PEG-SG hydrogels, due to its continuous crosslinking (Fig. 1E, Fig. S3), the preset printing pressure grew insufficient and frequent nozzle clogging occurred during printing. The printed structures shattered immediately after being immersed in PBS (Fig. 5C(ii)). For AHA/CMC hydrogel, due to the dehydration nature of the reversible Schiff base reaction, while the dynamic Schiff base linkages happen to be unstable in water [42], the filaments might fuse after only 3 min and result in bulk hydrogel (Fig. 5C (iii)). The results above demonstrated the time saving, time stability, and room temperature friendliness properties of the TSHSP hydrogel ink.

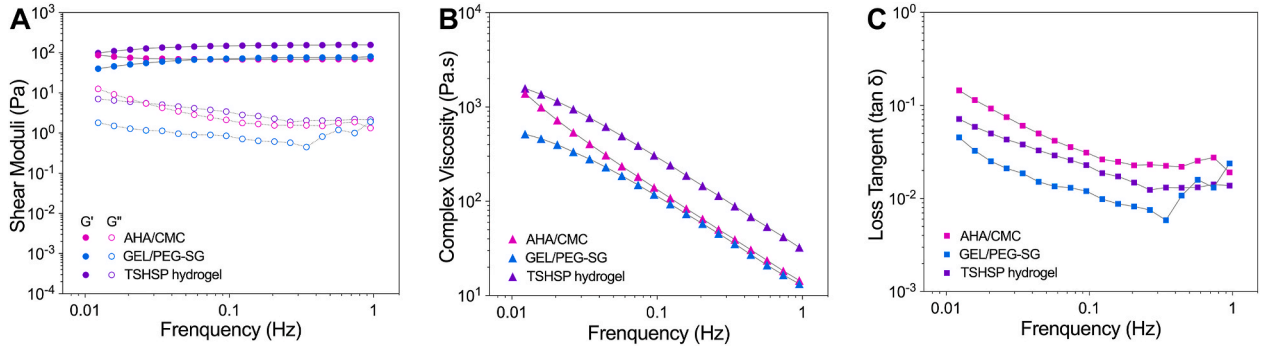

Fig. 3. Frequency dependence of shear moduli (A), |η*| (B), and tan δ (C) of AHA/CMC, GEL/PEG-SG, and TSHSP hydrogels.

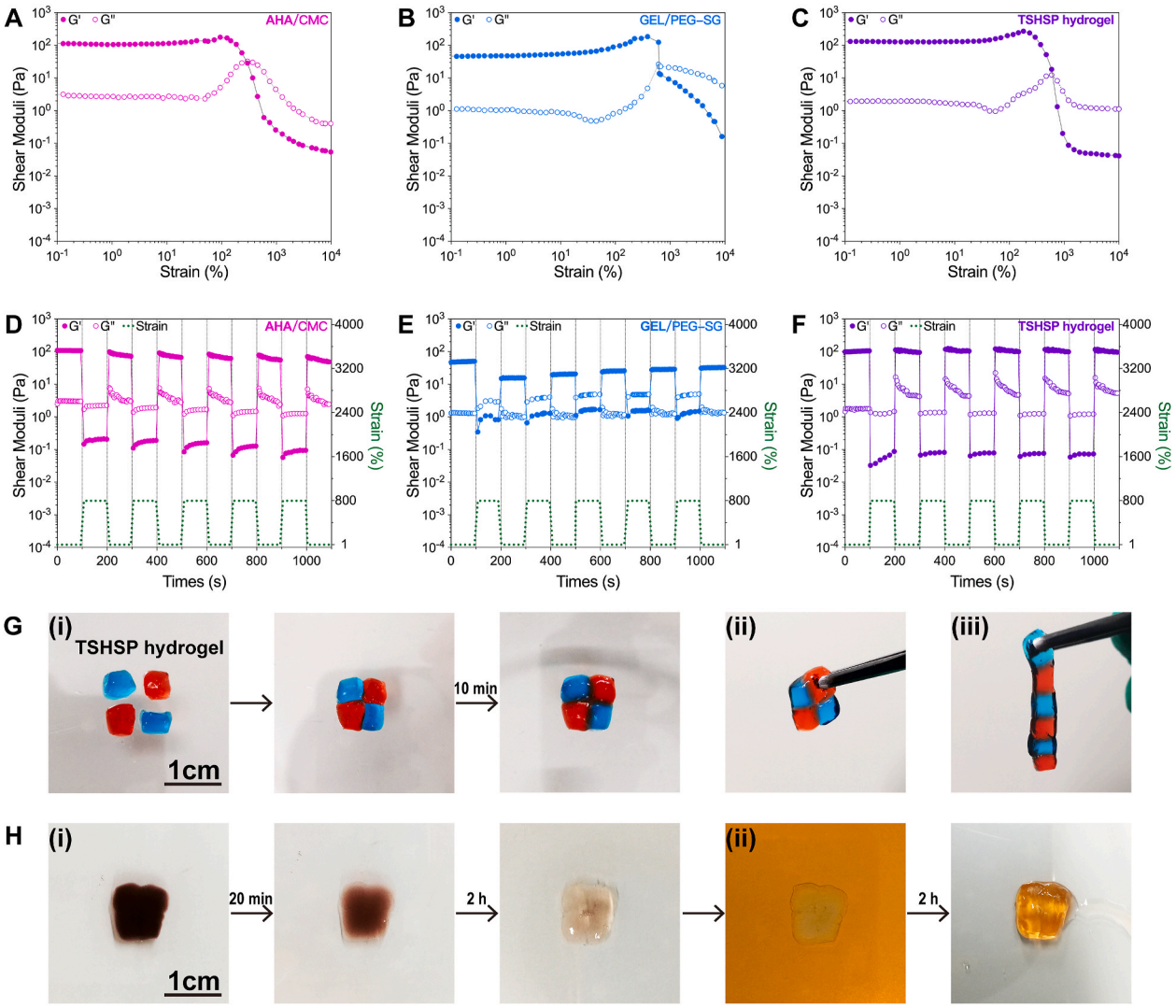

Fig. 4. Self-healing behavior and permeability of TSHSP hydrogel. (A)–(C) Response of AHA/CMC (A), GEL/PEG-SG (B), and TSHSP(C) hydrogels to increasing strains. (D)–(F) Recovery performance of AHA/CMC (D), GEL/PEG-SG (E), and TSHSP(F) hydrogels after repeated deformations. (G) Macroscopic self-healing behavior of TSHSP hydrogels (i), healed TSHSP hydrogels were lifted against their own weights (ii-iii). Hydrogels were stained with blue and red food dyes. (H) The dyes in the healed TSHSP hydrogel (fused after 4 h at room temperature) almost entirely escaped into PBS after 2 h at 37 °C (i), the new added yellow food dyes infiltrated into the hydrogel after another 2 h (ii). (For interpretation of the references to color in this figure legend, the reader is referred to the Web version of this article.)

3.5.2. *Subaqueous durability of cell-free constructs*

After further crosslinking with 4% (w/v%) PEG-SG solutions for 3 min, the cell-free constructs printed with TSHSP formulation were immersed in high glucose DMEM containing 10% FBS and incubated at 37 °C and 5% CO_2. Except for a few broken filaments on day 21, the entire structure manifested ample integrity during the entire incubation process (Fig. 5D). Moreover, we altered the proportion of the formulation for durability testing. To perform stable printing, we adjusted the volume ratio between AHA/CMC and GEL/PEG-SG without changing the concentration of the stock solutions. When the volume ratio of AHA, CMC, GEL, and PEG-SG stock solutions was 1:1:2:2 (final concentrations, 0.67% AHA, 0.5% CMC, 1.33% GEL, 0.67% PEG-SG), the sample maintained structural integrity within 7 days, after which the filaments began to break and completely shattered into pieces on day 14 (Fig. 5E). This is because the imine bonds of AHA/CMC were rapidly hydrolyzed at low concentrations and the non-healable amide bonds of GEL/PEG-SG could not maintain the integrity of the constructs at this time [23,27]. When we altered the volume ratio of AHA, CMC, GEL, and PEG-SG stock solutions to 2:2:1:1 (final concentrations, 1.33% AHA, 1% CMC, 0.67% GEL, 0.33% PEG-SG), for the same reason as the above, both AHA/CMC and low concentration GEL/PEG-SG were easily hydrolyzed. Therefore, the samples disappeared completely on day 14 (Fig. 5F). To continuously observe the printing fidelity and swelling ratio of the same sample, we used the linear expansion ratio (LER) instead of the traditional weight ratio. The ratio of the side length of the grid structure at different time points (SL_t) to the designed side length (SL_d) is LER. There was no difference in the printing fidelity and swelling ratio among the three formulations (Fig. 5G). In the formulation with the volume ratio of AHA, CMC, GEL, and PEG-SG being 1:1:1:1, the printing fidelity was 96.03 ± 2.36% just after printing and reached 122.27 ± 1.68% on day 21 (Fig. 5G).

3.6. *Cell viability and proliferation in bioprinted constructs*

We printed 6 layers of grid constructs with a size of 12 × 12 mm using the hydrogel bioink with NIH/3T3 cell concentration of 1.5×10^6/mL. Since the GEL/PEG-SG that contributes to stable structure support in TSHSP had not formed a completely stable cross-linked network just after printing (Fig. 1E and Fig. S3), 4% PEG-SG solutions were used for temporary construct reinforcement to avoid affecting the cell viability

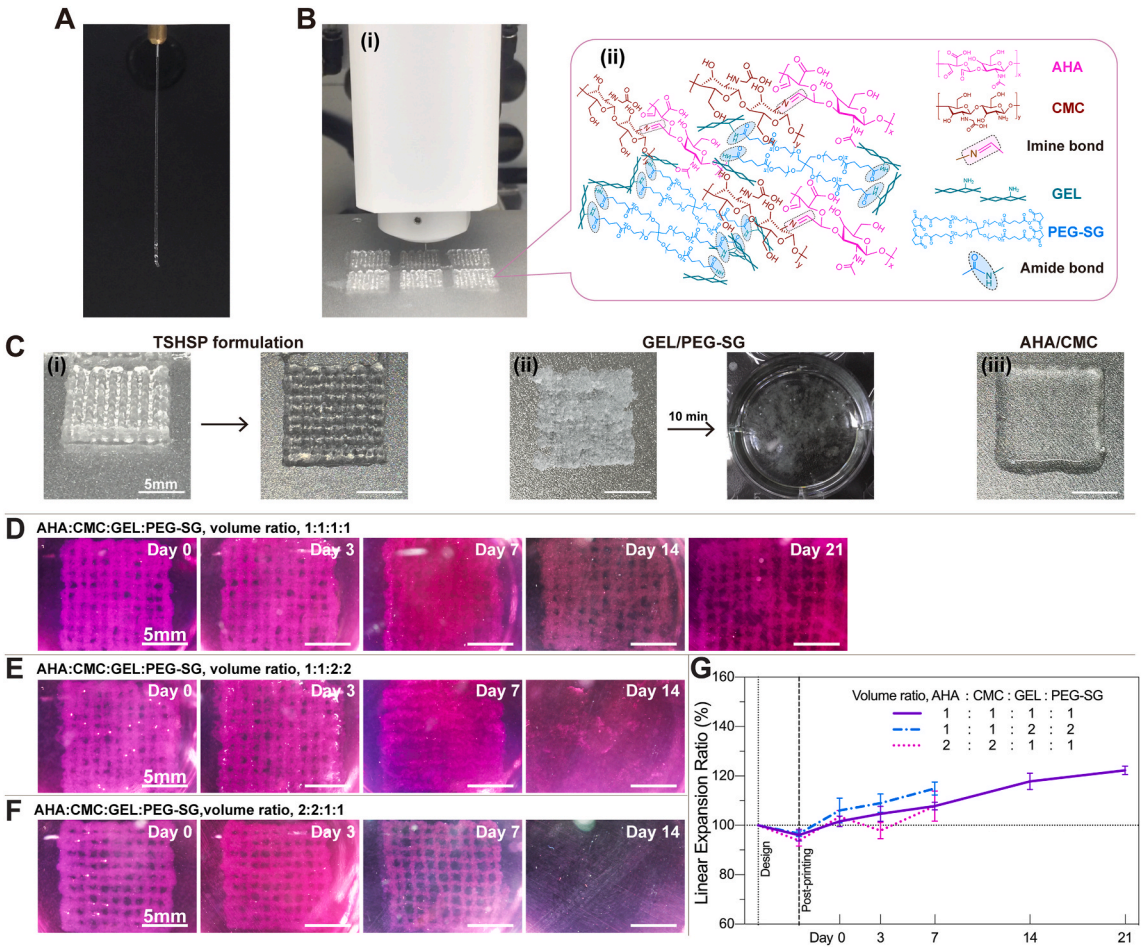

Fig. 5. Printability of TSHSP hydrogels and subaqueous durability of cell-free constructs. (A) Continuous extrusion of TSHSP hydrogel ink. (B) Printing of 6 grid structures at once with TSHSP ink (i) and schematic view of the gelation mechanism of TSHSP ink (ii). (C) Photographs of grid structure printed with TSHSP ink and its top view (i), laboriously printed non-integrated GEL/PEG-SG structure that shattered after being immersed in PBS for 10 min at room temperature (ii), and printed bulk AHA/CMC constructs (iii). (D)–(F) Subaqueous images of the integrity of cell-free constructs printed with different proportions of TSHSP formulations during incubation. (G) Printing fidelity and dimensional change profile of cell-free constructs compared to design (n = 3, error bars, mean ± SD).

due to the delay of cell-laden constructs culture. The GEL-ALG cell-laden constructs were cross-linked with 3% calcium chloride for 2 min as before [43].

3.6.1. Cell proliferation

Noticing from the proliferation profile of the Alamar Blue assay, cells in the TSHSP hydrogel constructs began to grow logarithmically on day 5, and entered a plateau on day 13, showing ample proliferation ability (Fig. 6A). While in GEL-ALG constructs, cells also began to grow logarithmically on day 5. However, the proliferation ability descended distinctly after reaching the peak on day 17, instead of entering a plateau (Fig. 6A). Under the more sensitive EdU DNA incorporation assay, the EdU^+ cells in TSHSP hydrogel constructs accounted for up to 43.59 ± 5.83% after a 12 h incubation on day 9 (Fig. 6B, (i, ii)), while the EdU^+ cells in GEL-ALG constructs were only 16.12 ± 2.67% (Fig. 6B, (i, iii)). On day 21, in the plateau of Alamar Blue assay, the proportion of EdU^+ cells in TSHSP hydrogel constructs was still as high as 12.35 ± 1.65% (Fig. 6B, (i, iv)), while the proportion in GEL-ALG was only 2.82 ± 1.28%, almost in a state of stagnant growth (Fig. 6B, (i, v)).

3.6.2. Cell viability

In TSHSP hydrogel constructs just printed (day 0), the proportions of live cells, dead cells, and live/dead dual-stained cells were 86.27 ± 4.18%, 0.45 ± 0.15%, and 9.18 ± 3.60%, respectively (Fig. 6, C and E), which shows no difference from the proportion of cells of the same type in GEL-ALG (90.94 ± 1.01%, 2.42 ± 1.44%, and 4.95 ± 0.40%, respectively) (Fig. 6D and E). On day 9, cells in TSHSP hydrogels manifested better viability (Fig. 6, C and E). The proportions of live cells and live/dead dual-stained cells in TSHSP hydrogel constructs were 93.83 ± 2.40% and 1.35 ± 0.54%, respectively (Fig. 6, C and E), while in GEL-ALG, the proportion of live cells decreased to 88.98 ± 1.94%, and the proportion of live/dead dual-stained cells increased to 9.22 ± 2.41% (Fig. 6D and E). On day 21, the proportion of live cells in TSHSP hydrogel constructs were still higher than that of GEL-ALG (89.97 ± 1.48% vs. 75.89 ± 2.73%), while the proportion of live/dead dual stained cells were still lower (2.27 ± 1.36% vs. 8.84 ± 0.31%, Fig. 6C–E). For dead cells, the percentages in the two constructs were all less than 0.7% on day 9 and 21, and there was no difference in these cell proportions between the two constructs on the same day (Fig. 6E). Especially on days 9 and 21, the dual staining of cells in GEL-ALG with calcein-AM and PI was not due to cell membrane damage caused by printing, but probably the early apoptosis caused by an unfavorable environment to cell growth (Fig. 6C–E). Moreover, the cell morphology in TSHSP hydrogel constructs began to expand on day 9 (Figs. 6C and S6), and fully expanded on day 21 (Fig. 6C(ii)), which is different from the pellet-like growth in GEL-ALG (Fig. 6D(ii)).

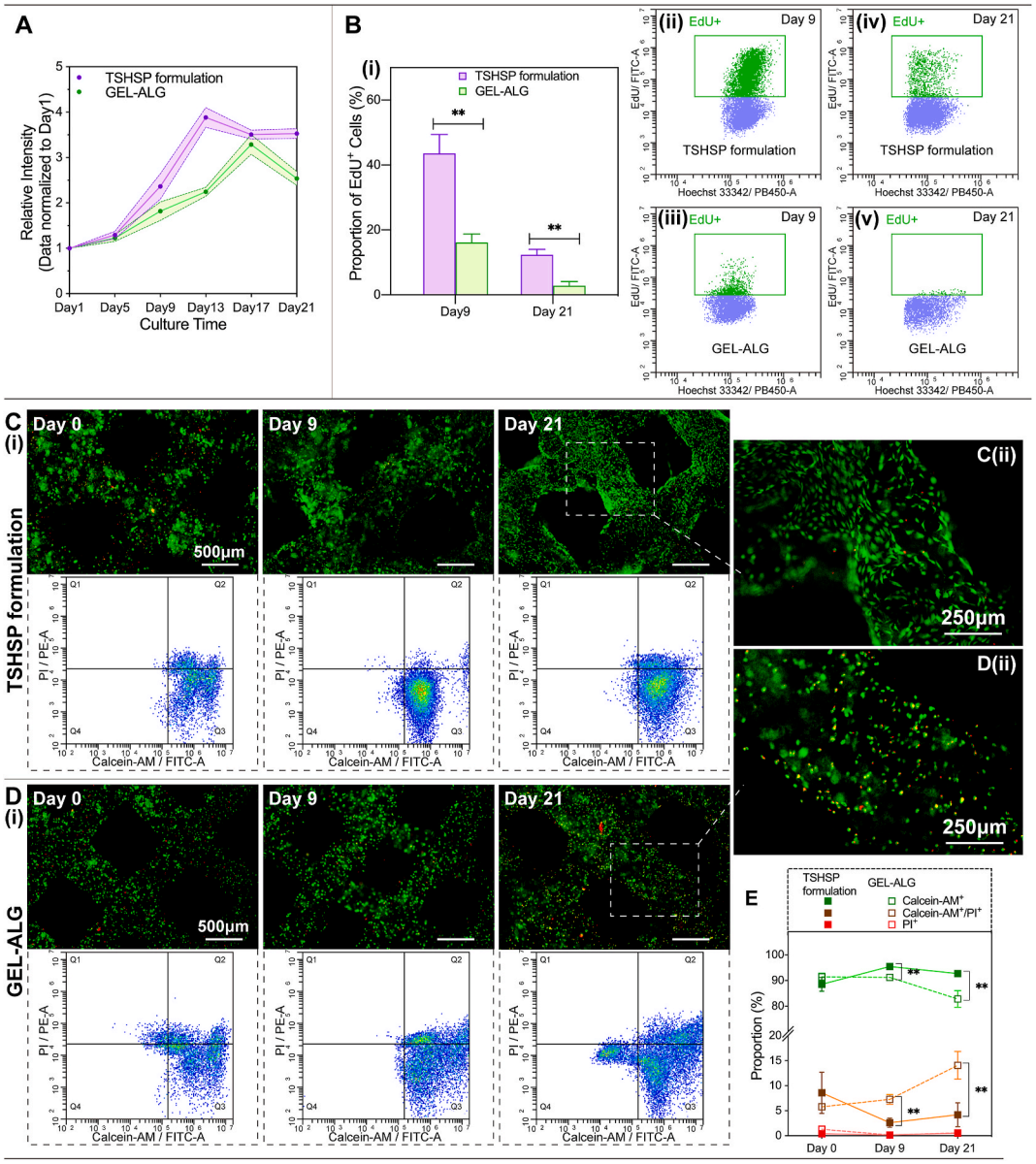

Fig. 6. Cell proliferation and viability performance of NIH/3T3 in bioprinted constructs. (A) Comparison of cell proliferation profiles in TSHSP hydrogel constructs and GEL-ALG constructs (Alamar Blue assay) (n = 3, error bars, mean ± SD). (B) Comparison of DNA replication in TSHSP hydrogel constructs and GEL-ALG constructs (i) (EdU incorporation assay) (n = 3, error bars, mean ± SD), cytometry plots of DNA replication in the above two constructs on day 9 and 29 (ii-v). (C)–(D) Micrographs and cytometry plots of live/dead stained cells in TSHSP hydrogel constructs (C) and GEL-ALG constructs (D). (E) Comparison of the changing trend of the proportion of cells in different states in the two constructs (n = 3, error bars, mean ± SD). $^{**}P < 0.01$, between different constructs at each time point. Cytometry plots of negative controls and positive controls were shown in Fig. S7. (For interpretation of the references to color in this figure legend, the reader is referred to the Web version of this article.)

3.7. Properties of in vitro tissue-like constructs

3.7.1. Macroscopic view of in vitro tissue-like constructs

All types of TSHSP hydrogel constructs manifested considerable integrity after 21 days of culture, which was different from the partial breakage of filaments in cell-free constructs (Fig. 7, A-C). A large number of cells can ensure sufficient extracellular matrix, which provides the foundation for the integrity of the constructs. Additionally, the C2C12 and chondrocyte constructs printed with the TSHSP formulation showed varying degrees of shrinkage. For C2C12 constructs, the shrinkage is related to the contraction behavior of cells after myogenic differentiation, while the construct without myogenic induction had no such change (Figs. 7B and S8). For chondrocyte constructs, the aggregate growth of chondrocytes in a three-dimensional environment led to the significant shrinkage of constructs [44], which in turn caused the disappearance of the primary micropores (Figs. 7C and S9).

3.7.2. Cell distribution of in vitro tissue-like constructs

We observed a large number of cells/cell clusters inside the microfilaments of all three *in vitro* tissue constructs (Fig. 7D–G). The density (%area of DAPI staining) of cells/cell clusters in these three TSHSP constructs were consistent with each other and more than that of GEL-ALG (Fig. 5G). Considering the consistent initial cell concentration of the same type of cells in TSHSP and GEL-ALG constructs, the higher % area of DAPI in the TSHSP constructs after 21 days of culture indicates that in addition to NIH/3T3, this new formulation is also more beneficial to the cell viability of NE-4C, C2C12, and chondrocytes. Moreover, the dispersion degree of cells/cell clusters was evaluated by CoV of %area of

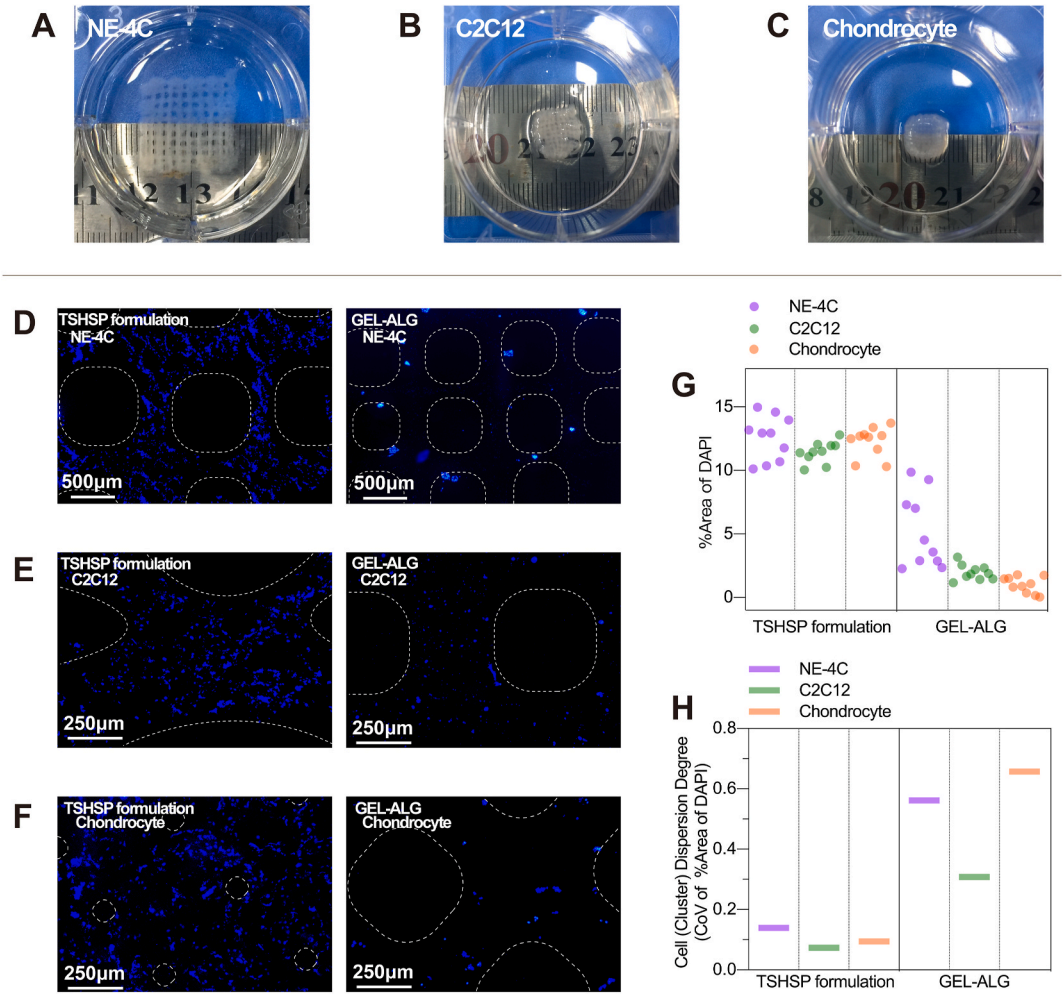

Fig. 7. Properties of *in vitro* tissue-like constructs after 21 days of culture. (A)–(C) Photographs of NE-4C (A), C2C12 (B), and Chondrocyte (C) constructs printed with TSHSP formulation after 21 days of culture. (D)–(F) Images of DAPI stained NE-4C (D), C2C12 (E), and chondrocyte (F) constructs. (G) Cell density and distribution plots of tissue-like constructs evaluated by DAPI staining (n = 10). (H) Cells/cell clusters dispersion degree plots of tissue-like constructs evaluated by CoV (SD/mean) of % area of DAPI. Dotted lines, microfilament range.

DAPI in different locations. The CoV of %area of DAPI of cells/cell clusters in three types of TSHSP constructs was lower than that of GEL-ALG constructs, indicating more homogenous cells/cell clusters distribution (Fig. 7H). Both the considerable density and homogeneity of different cells/cell clusters manifest the extensive applicability of TSHSP bioink formulation. According to literature, after the neuronal differentiation of neural stem cells (NE-4C) is induced by ATRA, the cells could show aggregate growth [45]. In NE-4C constructs based on the TSHSP formulation, cells in the microfilament grew homogeneously into string-like cell clusters (Fig. 7D). Although the NE-4C clusters in GEL-ALG constructs were larger, they were scarce in number and scattered near the surface of the microfilaments (Fig. 7D), suggesting insufficient matter exchange in the deep part of the constructs. In constructs printed with GEL-ALG bioinks, there were only sparse cell clusters and fewer cells (Fig. 7D–G), and the cells were un-uniformly distributed (Fig. 7H), making it less practical.

3.8. Immunohistological analyses of in vitro tissue-like constructs

3.8.1. NE-4C constructs

Corresponding to the distribution of NE-4C clusters, the immunoreactivity of nestin and βIII-tubulin was evenly shown in TSHSP hydrogel constructs, while sparsely shown in GEL-ALG constructs (Fig. 8A and B). Nestin is a critical marker of neural stem cells. In the process of differentiation of stem cells into neurons induced by ATRA, this immunoreactivity will gradually decrease, accompanied by cell aggregation [46]. The nestin immunoreactivity of cells in TSHSP hydrogel constructs was more distinguished than that in GEL-ALG (Fig. 8C), suggesting that NE-4C cells retain the characteristics of neural stem cells better, which means that the maturity of differentiated neurons was lower in these constructs [47]. However, the βIII-tubulin, a marker of neuron formation, its immunoreactivity in TSHSP hydrogel constructs was similar to that in GEL-ALG (Fig. 8C). Considering that after 21 days of culture, there were more cells/cell clusters in the TSHSP hydrogel construct with the same amount of initial cells as the GEL-ALG construct, we suppose this is related to the continued proliferation of undifferentiated cells in the subsequent culture after induction. In GEL-ALG constructs, the renewal of undifferentiated stem cells was limited. Therefore, the increase of tubulin's immunoreactivity was at the expense of nestin's immunoreactivity (Fig. 8C). For the TSHSP hydrogel construct, its good performance in terms of both proliferation and differentiation is more attractive for nerve regeneration.

3.8.2. C2C12 constructs

Desmin and myosin are two important markers in the intermediate and late stages of myogenic differentiation [48–50]. Similar to NE-4Cs, C2C12s in TSHSP hydrogel constructs also showed positive myogenic markers consistent with the distribution of cells/cell clusters (Fig. 8D

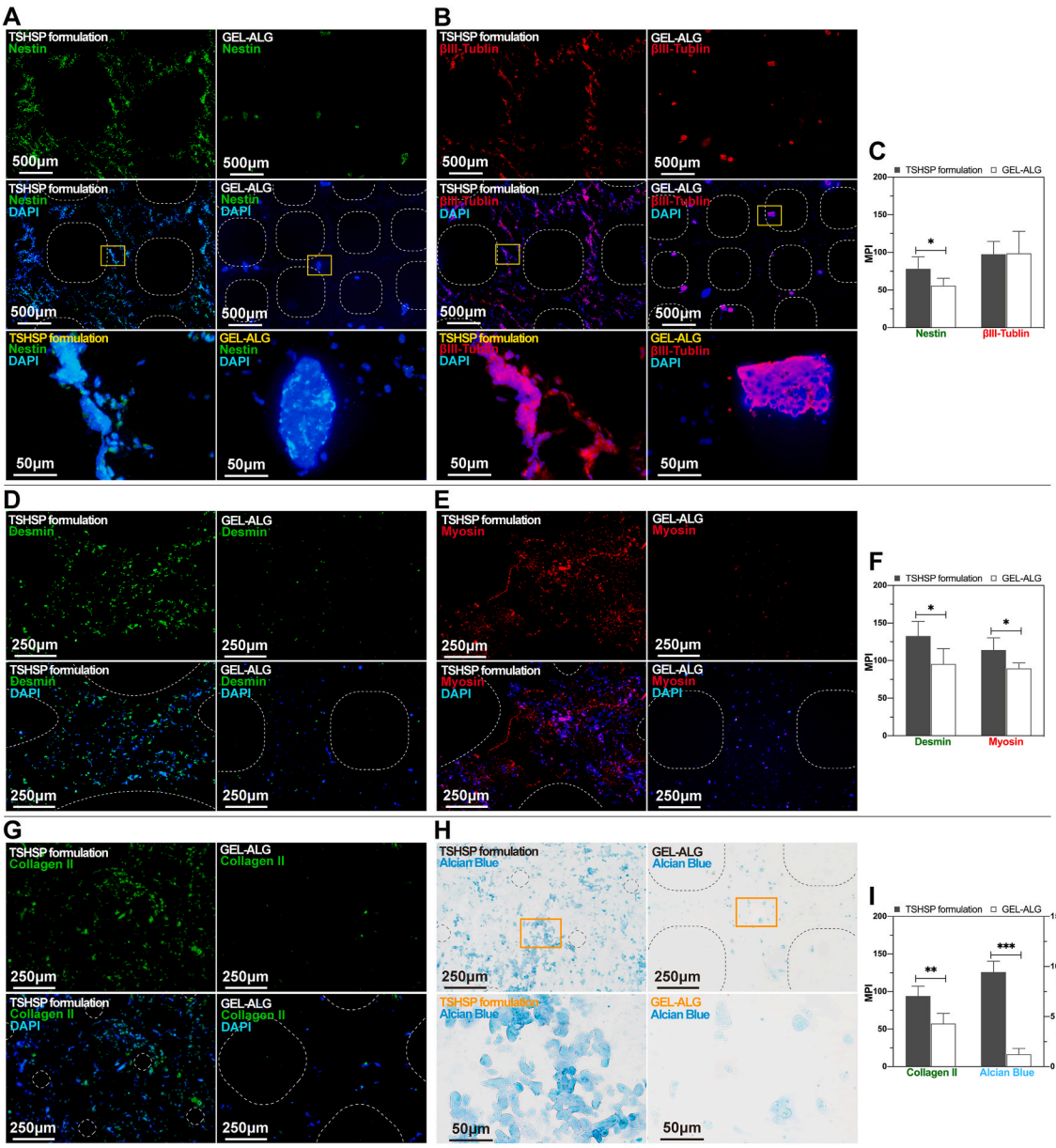

Fig. 8. Immunohistological images and semi-quantitative analyses of specific markers of *in vitro* tissue-like constructs after 21 days of culture. (A)–(C) Nestin and tublin staining in NE-4C constructs and semi-quantitative analyses of their immunoreactivity (n = 5, error bars, mean ± SD). (D)–(F) Desmin and fast myosin skeletal heavy chain staining in C2C12 constructs and semi-quantitative analyses of their immunoreactivity (n = 5, error bars, mean ± SD). (G)–(I) Collagen II and alcian blue staining in chondrocyte constructs and their semi-quantitative analyses (n = 5, error bars, mean ± SD). Yellow and orange squares: the position of the high-magnification images below. Dotted lines, microfilament range. $^{*}P < 0.05$, $^{**}P < 0.01$, $^{***}P < 0.001$, between different constructs. Images of negative controls were shown in Fig. S11. (For interpretation of the references to color in this figure legend, the reader is referred to the Web version of this article.)

and E). The immunoreactivity of desmin and fast myosin skeletal heavy chain were both more active than those in GEL-ALG constructs (Fig. 8F). This more effective and uniform differentiation provides a better option for muscle repair. Since C2C12 cells can inherently express a certain degree of desmin, the cells in uninduced TSHSP hydrogel constructs were positive for desmin staining and negative for myosin staining (Fig. S10). Since the uninduced TSHSP hydrogel constructs did not shrink as induced constructs (Fig. S8), we suppose that the myosin had been involved in cell contraction, leading to the shrinkage of induced muscle-like structures, although myotubes had not yet formed.

3.8.3. *Chondrocyte constructs*

The cell-cell interaction after chondrocyte aggregation plays a vital role in cartilage tissue engineering [44]. In the chondrocyte constructs printed with TSHSP bioink, the characteristic collagen II and sulfated glycosaminoglycans accumulate more significantly with the presence of a large number of cell clusters (Fig. 8, G-I). The shrinkage of constructs can help to provide a hypoxic microenvironment suitable for cartilage engineering [51]. However, hypoxia is not an independent factor that promotes cartilage regeneration, which requires proper extracellular matrix, nutrition, and paracrine of cell clusters as the basis [51–53]. Therefore, these factors were more balanced than that of GEL-ALG due to the presence of HA, high permeability, and significant cell aggregation in constructs based on TSHSP formulation.

4. Discussion

For 3D bioprinting, hydrogels based on dynamic chemical bonds can

prevent the printed filaments from breaking, while hydrogels with stable chemical bonds have the advantage of stability [3]. In this work, we applied the respective advantages of the above two types of hydrogels to establish the TSHSP bioink system based on the TSH strategy. Meanwhile, hydrogels containing HA and GEL can mimic the extracellular environment well [23,54,55]. Therefore, it is often used for 3D cell culture and most tissue engineering [56–58].

In this formulation, the AHA/CMC system achieves gelation through the Schiff base linkage between the amino of CMC and the aldehyde of AHA, and the GEL/PEG-SG system realizes gelation through the reaction between the amines of GEL and the succinimidyl esters of PEG-SG [22,26,59]. These two gelation systems have been proven effective in many aspects of biomanufacturing [20,23]. With balanced viscoelasticity provided by the dual crosslinked interpenetrating macromolecular network, the TSHSP hydrogel performed well in printing [4]. The G′ and failure strain did not increase geometrically because of the double dilution effect of each component when the two systems were mixed (Figs. 1F and 4C).

In this work, the fast gelation and dynamic imine bonds of AHA/CMC hydrogels enabled direct printing after bioink preparation. Due to the dehydration nature of the reversible Schiff base reaction and the instability of dynamic imine bond in water, the partial healing behavior of AHA/CMC hydrogel in rheological tests was not the incomplete recovery after deformation, but the reduction of G′ caused by the hydrolysis of the imine bond [42]. It is also for this reason that the AHA/CMC constructs fused into bulk hydrogels within 3 min after printing (Fig. 5C(iii)). Due to the superior self-healing capacity of Schiff base hydrogels, printed structures usually have large primary pores, which makes it difficult to ensure sufficient microstructure. Otherwise, complex methods or additional agents were required to achieve printing [60–62]. For GEL/PEG-SG system, although the stable amide bonds were destroyed inevitably during printing, the slow gelation of the system continued to occur after destructive deformation (Fig. 4E and Fig. S3). This continuous compensation effect for the loss of AHA/CMC storage modulus made the TSHSP hydrogel exhibited a ‘pseudo’ self-healing property in rheological testing (Fig. 4F). However, in the macroscopic healing testing, the TSHSP hydrogel performed a ‘real’ self-healing behavior (Fig. 4G). In printing, the proper self-healing ability of the new hydrogel not only avoided the fusion phenomenon when the AHA/CMC system was used alone but also ensured the integrity and durability of the printed constructs (Figs. 5D and 6C). Moreover, the TSHSP hydrogel can be used for printing at room temperature, which improves the convenience of printing compared with bioinks that rely on the temperature response of GEL [2,23].

We confirmed through macroscopic and rheological tests that the AHA/CMC and the GEL/PEG-SG play essential roles in the gelation of TSHSP hydrogel (Fig. 1D–I). The gelation of macromolecules is closely related to the length and spatial structure of the molecular chain, active group proportion, solution concentration, pH value, temperature, etc [26,63,64]. For AHA and GEL, the proportion of free amino in GEL is not as much as that in CMC, and the Schiff base reaction occurred more slowly at similar concentrations. Therefore, they were mainly used for auxiliary gelation [65]. On the other hand, molecular chains are not easy to entangle due to their lower crosslinking efficiency, and the realization of gelation usually required a longer reaction time (over 12 h), higher concentrations of GEL (10%), and extra crosslinkers [63,66,67]. For CMC and PEG-SG, the low gelation efficiency is due to the lower molecular weight of PEG, the lower concentration of both in our formulation, and the less prone the molecular chains of CMC to entangle like GEL [26,63,64]. Therefore, it is not easy for CMC and PEG-SG to form supramolecular networks. CMC-PEG hydrogels are usually obtained by applying other types of PEG derivatives or by using functionalized PEG just as a co-crosslinker [68,69]. Although succinimidyl active ester functionalized PEG is apt to crosslink with protein-based amino, the gelation is still slow [22]. Ideal hydrogels were often obtained by increasing the GEL concentration, reaction time, and temperature [22,23]. In 3D bioprinting, the gelation system based on GEL and succinimidyl active ester functionalized PEG was usually used in the form of a lightly crosslinked hydrogel, and the shape maintenance during printing also relied on low temperature [23]. In this work, the high molecular weight PEG-SG shortened the structure-supporting gelation time to < 1 h (Fig. S3, Table 1 and Table S1). However, the time-limited windows for structure-supporting printing were too short to be controlled, and due to the non-healable nature of amide bonds in GEL/PEG-SG, the construct fragmented into hydrogel pieces even when we performed post-printing reinforcement with 4% PEG-SG (Fig. 5C(ii)). The unfriendliness of this system exceedingly limits its application in bioprinting.

In the printing of hydrogels with interpenetrating networks, stiff crosslinks are disrupted during deformation, while the flexible covalent crosslinks help maintain structural integrity [4]. During the gelation of GEL/PEG-SG, the G′ didn’t reach the maximum even after 1 h of reaction (Fig. S3), which made the internal supramolecular network continue to be generated even after printing. Therefore, with the post-printing reinforcement under a shorter time (3 min) and a low concentration (4% PEG crosslinker) compared with other reports (10 min, 10% PEG crosslinker) [15], the cell-free constructs did not show partial filament breakage until day 21. For the cell-laden constructs under the same time, they still maintained integrated structures due to their rich extracellular matrix and cell-cell connections. In addition, the enzymatic stability of the chemical bonds that form the interpenetrating network is also critical for tissue repair. In our formulation, the stable amide bonds of GEL/PEG-SG exist naturally in the epithelial, muscle, and cartilage tissues of mammals that can secrete endogenous collagenase, which provides a biological basis for its enzymatic stability in human tissues.

Achieving high cell viability requires an outstanding hydrophilic microenvironment. The biomaterials in our formulation are not only hydrophilic but also water retentive [70], making cell viability and proliferation both impressive. The hydrophilicity and hierarchical pore structures of printed hydrogels provide the material and structural basis for its permeability, which is essential for maintaining the viability of deep cells. It took ~2 h for the food dye to completely permeate the bulk hydrogel macroscopically (Fig. 4H), while reported macroscopic permeation of alginate or PEG-based hydrogel took weeks or required additional assistance to complete [71,72]. In the later stage of the culture, the proportion of dual stained cells was <5% in Live/Dead staining (Fig. 6, C and E), and high-concentration cells distributed homogeneously in the tissue-like constructs (Fig. 7D–H), which indicates that this new type of hydrogel bioink can ensure nutrients and oxygen delivery probably by maintaining high permeability. In low-stiffness hydrogels, cells spread well and showed preferable interconnection [73]. The G′ of TSHSP hydrogel is ~100 Pa (Fig. 4F), which is a suitable low value that can meet the structure-supporting requirement and fall into the ideal soft hydrogel range [23]. Therefore, NIH/3T3 manifested a noteworthy spreading of cell morphology (Fig. 6C), while cells in tissue-like constructs exhibited considerable cell-cell interconnections (Fig. 7, D-F).

The strong permeability of the TSHSP hydrogel ensured equal opportunities for cells to obtain nutrients and stay away from metabolic waste, thereby ensuring considerable cell viability, proliferation, and cell-cell interconnections, regardless of the cell locations or types in constructs. Therefore, in tissue-like constructs, the cell/cell clusters manifested uniform distribution and biological specificities, making these constructs suitable for homogenous tissue repair and regeneration (Figs. 7 and 8).

Nerve, muscle, and articular cartilage-related injuries and diseases are common reasons of reduced quality of life. Therefore, we selected NE-4C, C2C12, and chondrocytes to evaluate the effects of TSHSP hydrogel in the corresponding *in vitro* constructs. For the NE-4C nerve-like constructs, the high permeability of TSHSP hydrogel ensured the equal induction of NE-4C cells. The hypoxic microenvironment of the cell clusters can also facilitate neurogenesis [74]. With the above neural

differentiation-related factors, the related marker was expressed uniformly in each cell cluster. It is known that cell contact communication is essential for neural differentiation and the functionalization of neural tissue constructs [75]. Therefore, the properties of the NE-4C constructs ensured a structural foundation for communication between cells or cell clusters, making this bioink suitable for *in vitro* neurogenesis and have the potential for nerve tissue repair. The cells in GEL-ALG constructs only aggregated near the surface of printed filaments. Although the cell clusters had undergone neural differentiation due to the initiation of ATRA (Fig. 8B), it was not easy for the sparse cell clusters to communicate with each other, making GEL-ALG inferior to the TSHSP bioink in terms of nerve tissue repair. In addition to cell distribution, appropriate mechanical external force and extracellular matrix are also beneficial to myogenesis [50,76,77]. In this work, we mainly focused on the biological behavior of cells in the new bioink. Therefore, we did not apply decellularized extracellular matrix or external force stimuli (such as stretching) as in other reports, resulting no myotubes occurrence in our models [50,76,77]. For cartilage engineering, in addition to the above factors, the autocrine effect of cells, which depends on the direct interaction of cell-cell and cell-extracellular matrix, also promotes cartilage regeneration by increasing the size of cell clusters [78]. Therefore, the excessively sparse cells and cell clusters caused by weak cell viability and proliferation in GEL-ALG constructs led to insufficient extracellular matrix secretion (Fig. 8, G-I).

As the main components of the extracellular matrix, HA and proteins play an important role in tissue regeneration and repair. This biomimetic hydrogels has been used for research or application of brain [57,79], liver [80], muscle [81,82], skin [58] and cartilage [17,83] tissue engineering. Therefore, in addition to the permeability, HA and GEL in TSHSP bioink also contributed to the remarkable biological specificities of *in vitro* tissue-like constructs. Moreover, the reaction of succinimidyl active ester functionalized PEG with protein-based amino groups makes the hydrogel easier to integrate with recipient tissues, and chitosan has natural antibacterial properties because of its cationic interference with bacterial metabolism [21,84,85]. These also make the TSHSP bioink-based tissue-like constructs beneficial for tissue repair. In the future, we will further optimize the TSHSP bioink in terms of strength, durability, degradability, biological activity, cell behavior, and repair capability according to tissue-specific requirements, and to implement more comprehensive biomimetic manufacturing and evaluation of specific *in vitro* tissue-like constructs or organoids based on this bioink system.

The limitation of this study is that the unassisted structural support of the TSHSP formulation was only achieved during the printing process, although this did improve the convenience of printing effectively. Since the stable network of GEL/PEG-SG had not been fully formed just after printing, an additional post-printing reinforcement was still required to perform cell-laden construct culture as soon as possible. It is still a challenge to achieve completely unassisted structural support in printing, cultivation, and application. In the future, we will further optimize the TSHSP formulation to realize more considerable practical value in bioprinting.

5. Conclusion

In this work, we present the TSHSP bioink by simply mixing a fast AHA/CMC gelation system with dynamic covalent bonds and a slow GEL/PEG-SG gelation system with stable covalent bonds. The TSH property of the bioink enables room-temperature printing just after formulation preparation, avoids breaking printed filaments, realizes uniform printing of integrated structure-supporting constructs, ensures the stability of shape and microstructure during printing and long-term durability of constructs during culture. The low stiffness, high water retention, high permeability, biocompatible components, and uniformly distributed cells of this bioink make the cell viability, cell morphology, and the biological specificities of tissue-like constructs perform well. We envision that this bioink can be used in a variety of soft tissue engineering in the future, as well as in the form of cell carriers for hard tissue engineering combining with high-strength materials or for targeted cell therapy. Additionally, the TSH strategy of this bioink can provide a method for applying other gelation systems to develop the gel-phase bioinks or cell-carriers with similar requirements.

CRediT authorship contribution statement

Hongqing Chen: Conceptualization, Methodology, Investigation, Data curation, Formal analysis, Visualization, Writing – original draft. **Fei Fei:** Methodology, Investigation, Data curation, Validation, Visualization, Writing – original draft. **Xinda Li:** Methodology, Investigation, Data curation, Validation, Writing – review & editing. **Zhenguo Nie:** Investigation, Data curation, Visualization. **Dezhi Zhou:** Investigation, Resources. **Libiao Liu:** Methodology, Software. **Jing Zhang:** Resources, Validation. **Haitao Zhang:** Resources, Visualization. **Zhou Fei:** Conceptualization, Writing – review & editing, Supervision, Project administration, Funding acquisition. **Tao Xu:** Conceptualization, Methodology, Writing – review & editing, Supervision, Project administration, Funding acquisition.

Declaration of competing interest

We declare that we have no financial and personal relationships with other people or organizations that can inappropriately influence our work. There is no professional or other personal interest of any nature or kind in any product, service and/or company that could be construed as influencing the position presented in, or the review of the manuscript entitled "**A structure-supporting, self-healing, and high permeating hydrogel bioink for establishment of diverse homogeneous tissue-like constructs**".

Acknowledgments

We thank **Zhizhong Jin** for his help in bioprinting of cell-laden constructs, **Lidan Chen** for her help in flow cytometry analysis, **Cheng Ma** for providing suggestions on the optimization of AHA synthesis and TSHSP formulation.

Appendix A. Supplementary data

Supplementary data to this article can be found online at https://doi.org/10.1016/j.bioactmat.2021.03.019.

Funding

This work was supported by the National Natural Science Foundation of China [grant number 52075285]; the Science and Technology Program of Guangzhou, China [grant number 201604040002]; the Key-Area Research and Development Program of Guangdong Province, China [grant number 2020B090923003]; and the Key Research and Development Projects of People's Liberation Army, China [grant number. BWS17J036].

References

[1] S.V. Murphy, A. Atala, 3D bioprinting of tissues and organs, Nat. Biotechnol. 32 (2014) 85–773.
[2] L. Gasperini, J.F. Mano, R.L. Reis, Natural polymers for the microencapsulation of cells, J. R. Soc. Interface 11 (2014) 20140817.
[3] J.L. Mann, A.C. Yu, G. Agmon, E.A. Appel, Supramolecular polymeric biomaterials, Biomater. Sci. 6 (2017) 10–37.
[4] D. Chimene, R. Kaunas, A.K. Gaharwar, Hydrogel bioink reinforcement for additive manufacturing: a focused review of emerging strategies, Adv. Mater. 32 (2019) 1902026.

[5] L. Ouyang, R. Yao, S. Mao, X. Chen, J. Na, W. Sun, Three-dimensional bioprinting of embryonic stem cells directs highly uniform embryoid body formation, Biofabrication 7 (2015) 1–12.

[6] M. Costantini, J. Idaszek, K. Szöke, J. Jaroszewicz, M. Dentini, A. Barbetta, J. E. Brinchmann, W. Święszkowski, 3D Bioprinting of BM-MSCs-loaded ECM biomimetic hydrogels for in vitroneocartilage formation, Biofabrication **8** (2016) 35002.

[7] J.P.K. Armstrong, M. Burke, B.M. Carter, S.A. Davis, A.W. Perriman, 3D bioprinting using a templated porous bioink, Adv. Healthc. Mater. 5 (2016) 30–1724.

[8] K. Dubbin, Y. Hori, K.K. Lewis, S.C. Heilshorn, Dual-stage crosslinking of a gel-phase bioink improves cell viability and homogeneity for 3D bioprinting, Adv. Healthc. Mater. 5 (2016) 92–2488.

[9] S.A. Wilson, L.M. Cross, C.W. Peak, A.K. Gaharwar, Shear-thinning and thermo-reversible nanoengineered inks for 3D bioprinting, ACS Appl. Mater. Interfaces 9 (2017) 58–43449.

[10] C.B. Highley, C.B. Rodell, J.A. Burdick, Direct 3D printing of shear-thinning hydrogels into self-healing hydrogels, Adv. Mater. 27 (2015) 9–5075.

[11] D.M. Kirchmajer, R. Gorkin III, M. Panhuis, An overview of the suitability of hydrogel-forming polymers for extrusion-based 3D-printing, J. Mater. Chem. B 3 (2015) 17–4105.

[12] L. Ouyang, C.B. Highley, W. Sun, J.A. Burdick, A generalizable strategy for the 3D bioprinting of hydrogels from nonviscous photo-crosslinkable inks, Adv. Mater. 29 (2016) 1604983.

[13] D.E. Godar, C. Gurunathan, I. Ilev, 3D bioprinting with UVA1 radiation and photoinitiator irgacure 2959: can the ASTM standard L929 cells predict human stem cell cytotoxicity? Photochem. Photobiol. 95 (2018) 6–581.

[14] A. Skardal, M. Devarasetty, H.-W. Kang, I. Mead, C. Bishop, T. Shupe, S.J. Lee, J. Jackson, J. Yoo, S. Soker, A. Atala, A hydrogel bioink toolkit for mimicking native tissue biochemical and mechanical properties in bioprinted tissue constructs, Acta Biomater. 25 (2015) 24–34.

[15] A.L. Rutz, E.S. Gargus, K.E. Hyland, P.L. Lewis, A. Setty, W.R. Burghardt, R. N. Shah, Employing PEG crosslinkers to optimize cell viability in gel phase bioinks and tailor post printing mechanical properties, Acta Biomater. 99 (2019) 32–121.

[16] C. Loebel, C.B. Rodell, M.H. Chen, J.A. Burdick, Shear-thinning and self-healing hydrogels as injectable therapeutics and for 3D-printing, Nat. Protoc. 12 (2017) 41–1521.

[17] H. Tan, C.R. Chu, K.A. Payne, K.G. Marra, Injectable in situ forming biodegradable chitosan-hyaluronic acid based hydrogels for cartilage tissue engineering, Biomaterials 30 (2009) 506–2499.

[18] H. Tan, J.P. Rubin, K.G. Marra, Injectable in situ forming biodegradable chitosan-hyaluronic acid based hydrogels for adipose tissue regeneration, Organogenesis 6 (2014) 80–173.

[19] L. Li, N. Wang, X. Jin, R. Deng, S. Nie, L. Sun, Q. Wu, Y. Wei, C. Gong, Biodegradable and injectable in situ cross-linking chitosan-hyaluronic acid based hydrogels for postoperative adhesion prevention, Biomaterials 35 (2014) 17–3903.

[20] S.W. Kim, D.Y. Kim, H.H. Roh, H.S. Kim, J.W. Lee, K.Y. Lee, Three-dimensional bioprinting of cell-laden constructs using polysaccharide-based self-healing hydrogels, Biomacromolecules 20 (2019) 6–1860.

[21] K. Hamamura, Y. Weng, J. Zhao, H. Yokota, D. Xie, PEG attachment to osteoblasts enhances mechanosensitivity, Biomed. Mater. 3 (2008), 025017.

[22] A. Song, A.A. Rane, K.L. Christman, Antibacterial and cell-adhesive polypeptide and poly(ethylene glycol) hydrogel as a potential scaffold for wound healing, Acta Biomater. 8 (2012) 41–50.

[23] A.L. Rutz, K.E. Hyland, A.E. Jakus, W.R. Burghardt, R.N. Shah, A multimaterial bioink method for 3D printing tunable, cell-compatible hydrogels, Adv. Mater. (Weinheim) 27 (2015) 14–1607.

[24] K.H. Bouhadir, D.S. Hausman, D.J. Mooney, Synthesis of cross-linked poly (aldehyde guluronate) hydrogels, Polymer 40 (1999) 84–3575.

[25] D.Y. Kim, H. Park, S.W. Kim, J.W. Lee, K.Y. Lee, Injectable hydrogels prepared from partially oxidized hyaluronate and glycol chitosan for chondrocyte encapsulation, Carbohydr. Polym. 157 (2017) 7–1281.

[26] V.B. Gavalyan, Synthesis and characterization of new chitosan-based Schiff base compounds, Carbohydr. Polym. 145 (2016) 37–47.

[27] H. Chen, J. Cheng, L. Ran, K. Yu, B. Lu, G. Lan, F. Dai, F. Lu, An injectable self-healing hydrogel with adhesive and antibacterial properties effectively promotes wound healing, Carbohydr. Polym. 201 (2018) 31–522.

[28] H.-C. Ge, D.-K. Luo, Preparation of carboxymethyl chitosan in aqueous solution under microwave irradiation, Carbohydr. Res. 340 (2005) 6–1351.

[29] J.-S. Baek, C.-W. Cho, Surface modification of solid lipid nanoparticles for oral delivery of curcumin: improvement of bioavailability through enhanced cellular uptake, and lymphatic uptake, Eur. J. Pharm. Biopharm. 117 (2017) 40–132.

[30] S. Shahraki, H.S. Delarami, F. Khosravi, R. Nejat, Improving the adsorption potential of chitosan for heavy metal ions using aromatic ring-rich derivatives, J. Colloid Interface Sci. 576 (2020) 79–89.

[31] M. Sadeghi, S. Hemmati, H. Hamishehkar, Synthesis of a novel superdisintegrant by starch derivatization with polysuccinimide and its application for the development of Ondansetron fast dissolving tablet, Drug Dev. Ind. Pharm. 42 (2016) 75–769.

[32] A.M. Pistorius, P.J. Groenen, W.J. De Grip, Infrared analysis of peptide succinimide derivatives, Int. J. Pept. Protein Res. 42 (1993) 7–570.

[33] S. Devouge, J. Conti, A. Goldsztein, E. Gosselin, A. Brans, M. Voué, J. De Coninck, F. Homblé, E. Goormaghtigh, J. Marchand-Brynaert, Surface functionalization of germanium ATR devices for use in FTIR-biosensors, J. Colloid Interface Sci. 332 (2009) 15–408.

[34] A. Jafari, A. Amirsadeghi, S. Hassanajili, N. Azarpira, Bioactive antibacterial bilayer PCL/gelatin nanofibrous scaffold promotes full-thickness wound healing, Int. J. Pharm. 583 (2020) 119413.

[35] Q. He, X. Sun, S. He, T. Wang, J. Zhao, L. Yang, Z. Wu, H. Sun, PEGylation of black kidney bean (Phaseolus vulgaris L.) protein isolate with potential functironal properties, Colloids Surf. B Biointerfaces 164 (2018) 89–97.

[36] D.M. Yu, G.L. Amidon, N.D. Weiner, A.H. Goldberg, Viscoelastic properties of poly (ethylene oxide) solution, J. Pharmaceut. Sci. 83 (1994) 9–1443.

[37] M.M. Alam, Y. Sugiyama, K. Watanabe, K. Aramaki, Phase behavior and rheology of oil-swollen micellar cubic phase and gel emulsions in nonionic surfactant systems, J. Colloid Interface Sci. 341 (2010) 72–267.

[38] E.A. Appel, F. Biedermann, U. Rauwald, S.T. Jones, J.M. Zayed, O.A. Scherman, Supramolecular cross-linked networks via host-guest complexation with cucurbit [8]uril, J. Am. Chem. Soc. 132 (2010) 60–14251.

[39] B.G. Soliman, G.C.J. Lindberg, T. Jungst, G.J. Hooper, J. Groll, T.B.F. Woodfield, K. S. Lim, Stepwise control of crosslinking in a one-pot system for bioprinting of low-density bioinks, Adv. Healthc. Mater. (2020) e1901544.

[40] I.A. Marozas, K.S. Anseth, J.J. Cooper-White, Adaptable boronate ester hydrogels with tunable viscoelastic spectra to probe timescale dependent mechanotransduction, Biomaterials 223 (2019) 119430.

[41] T. Gao, G.J. Gillispie, J.S. Copus, PR A K, Y.-J. Seol, A. Atala, J.J. Yoo, S.J. Lee, Optimization of gelatin-alginate composite bioink printability using rheological parameters: a systematic approach, Biofabrication 10 (2018), 034106.

[42] V. Ramanujam, C. Charlier, A. Bax, Observation and kinetic characterization of transient Schiff base intermediates by CEST NMR spectroscopy, Angew Chem. Int. Ed. Engl. 58 (2019) 12–15309.

[43] X. Dai, C. Ma, Q. Lan, T. Xu, 3D bioprinted glioma stem cells for brain tumor model and applications of drug susceptibility, Biofabrication **8** (2016) 45005.

[44] K.S. Furukawa, H. Suenaga, K. Toita, A. Numata, J. Tanaka, T. Ushida, Y. Sakai, T. Tateishi, Rapid and large-scale formation of chondrocyte aggregates by rotational culture, Cell Transplant. 12 (2003) 9–475.

[45] K. Schlett, E. Madarász, Retinoic acid induced neural differentiation in a neuroectodermal cell line immortalized by p53 deficiency, J. Neurosci. Res. 47 (1997) 15–405.

[46] M. Jelitai, M. Anderová, A. Chvátal, E. Madarász, Electrophysiological characterization of neural stem/progenitor cells during in vitro differentiation: study with an immortalized neuroectodermal cell line, J. Neurosci. Res. 85 (2007) 17–1606.

[47] K. Schlett, B. Herberth, E. Madarász, In vitro pattern formation during neurogenesis in neuroectodermal progenitor cells immortalized by p53-deficiency, Int. J. Dev. Neurosci. 15 (1997) 795–804.

[48] J.N. Artaza, S. Bhasin, C. Mallidis, W. Taylor, K. Ma, N.F. Gonzalez-Cadavid, Endogenous expression and localization of myostatin and its relation to myosin heavy chain distribution in C2C12 skeletal muscle cells, J. Cell. Physiol. 190 (2002) 9–170.

[49] D. Paulin, Z. Li, Desmin: a major intermediate filament protein essential for the structural integrity and function of muscle, Exp. Cell Res. 301 (2004) 1–7.

[50] M. Yeo, G. Kim, Micro/nano-hierarchical scaffold fabricated using a cell electrospinning/3D printing process for co-culturing myoblasts and HUVECs to induce myoblast alignment and differentiation, Acta Biomater. 107 (2020) 14–102.

[51] C.B. Foldager, A.B. Nielsen, S. Munir, M. Ulrich-Vinther, K. Søballe, C. Bünger, M. Lind, Combined 3D and hypoxic culture improves cartilage-specific gene expression in human chondrocytes, Acta Orthop. 82 (2011) 40–234.

[52] W. Yan, X. Xu, Q. Xu, Z. Sun, Q. Jiang, D. Shi, Platelet-rich plasma combined with injectable hyaluronic acid hydrogel for porcine cartilage regeneration: a 6-month follow-up, Regen. Biomater. **7** (2019) 77–90.

[53] K. Gelse, M. Brem, P. Klinger, A. Hess, B. Swoboda, F. Hennig, A. Olk, Paracrine effect of transplanted rib chondrocyte spheroids supports formation of secondary cartilage repair tissue, J. Orthop. Res. 27 (2009) 25–1216.

[54] G.-K. Tan, D.L.M. Dinnes, L.N. Butler, J.J. Cooper-White, Interactions between meniscal cells and a self assembled biomimetic surface composed of hyaluronic acid, chitosan and meniscal extracellular matrix molecules, Biomaterials **31** (2010) 18–6104.

[55] S.C. Owen, S.A. Fisher, R.Y. Tam, C.M. Nimmo, M.S. Shoichet, Hyaluronic acid click hydrogels emulate the extracellular matrix, Langmuir 29 (2012) 400–7393.

[56] M.H. Asim, S. Silberhumer, I. Shahzadi, A. Jalil, B. Matuszczak, A. Bernkop-Schnürch, S-protected thiolated hyaluronic acid: in-situ crosslinking hydrogels for 3D cell culture scaffold, Carbohydr. Polym. 237 (2020) 116092.

[57] F. Li, M. Ducker, B. Sun, F.G. Szele, J.T. Czernuszka, Interpenetrating polymer networks of collagen, hyaluronic acid, and chondroitin sulfate as scaffolds for brain tissue engineering, Acta Biomater. 112 (2020) 35–122.

[58] M. Movahedi, A. Asefnejad, M. Rafienia, M.T. Khorasani, Potential of novel electrospun core-shell structured polyurethane/starch (hyaluronic acid) nanofibers for skin tissue engineering: in vitro and in vivo evaluation, Int. J. Biol. Macromol. 146 (2020) 37–627.

[59] A.J. Kuijpers, G.H. Engbers, J. Krijgsveld, S.A. Zaat, J. Dankert, J. Feijen, Cross-linking and characterisation of gelatin matrices for biomedical applications, J. Biomater. Sci. Polym. Ed. 11 (2000) 225–243.

[60] M. Weis, J. Shan, M. Kuhlmann, T. Jungst, J. Teßmar, J. Groll, Evaluation of hydrogels based on oxidized hyaluronic acid for bioprinting, Gels **4** (2018).

[61] J. Xu, Y. Liu, S.-H. Hsu, Hydrogels based on Schiff base linkages for biomedical applications, Molecules **24** (2019).

[62] M. Puertas-Bartolomé, M.K. Włodarczyk-Biegun, A. del Campo, B. Vázquez-Lasa, J. San Román, 3D printing of a reactive hydrogel bio-ink using a static mixing tool, Polymers **12** (2020).

[63] J.B. Rose, S. Pacelli, A.J.E. Haj, H.S. Dua, A. Hopkinson, L.J. White, F.R.A.J. Rose, Gelatin-based materials in ocular tissue engineering, Materials 7 (2014) 3106–3135.
[64] J.W. Seo, S.R. Shin, Y.J. Park, H. Bae, Hydrogel production platform with dynamic movement using photo-crosslinkable/temperature reversible chitosan polymer and stereolithography 4D printing Technology, Tissue Eng. Regen. Med. 45 (2020) 9–286.
[65] J. Chen, X. Wang, H. Ye, Z. Yu, L. Feng, J. Zhou, Y. Che, Fe (III)@TA@IGF-2 microspheres loaded hydrogel for liver injury treatment, Int. J. Biol. Macromol. 159 (2020) 93–183.
[66] L. Weng, H. Pan, W. Chen, Self-crosslinkable hydrogels composed of partially oxidized hyaluronan and gelatin: in vitro and in vivo responses, J. Biomed. Mater. Res. 85 (2008) 65–352.
[67] J.-Y. Lai, D.H.-K. Ma, Ocular biocompatibility of gelatin microcarriers functionalized with oxidized hyaluronic acid, Mater. Sci. Eng. C Mater. Biol. Appl. 72 (2017) 9–150.
[68] W. Huang, Y. Wang, Y. Chen, Y. Zhao, Q. Zhang, X. Zheng, L. Chen, L. Zhang, Strong and rapidly self-healing hydrogels: potential hemostatic materials, Adv. Healthc. Mater. 5 (2016) 22–2813.
[69] K. Wang, S. Lin, K.C. Nune, R.D.K. Misra, Chitosan-gelatin-based microgel for sustained drug delivery, J. Biomater. Sci. Polym. Ed. 27 (2016) 53–441.
[70] L. Håkansson, R. Hällgren, P. Venge, Regulation of granulocyte function by hyaluronic acid. In vitro and in vivo effects on phagocytosis, locomotion, and metabolism, J. Clin. Invest. 66 (1980) 298–305.
[71] R.W. Chakroun, A. Sneider, C.F. Anderson, F. Wang, P.H. Wu, D. Wirtz, H. Cui, Supramolecular design of unsymmetric reverse bolaamphiphiles for cell-sensitive hydrogel degradation and drug release, Angew. Chem. Int. Ed. 59 (2020) 4434–4442.
[72] X. Wei, C. Liu, Z. Wang, Y. Luo, 3D printed core-shell hydrogel fiber scaffolds with NIR-triggered drug release for localized therapy of breast cancer, Int. J. Pharm. 580 (2020) 119219.
[73] J. Zhang, E. Wehrle, J.R. Vetsch, G.R. Paul, M. Rubert, R. Müller, Alginate dependent changes of physical properties in 3D bioprinted cell-laden porous scaffolds affect cell viability and cell morphology, Biomed. Mater. 14 (2019), 065009.
[74] X. Li, X. Wang, H. Chen, Z. Jin, X. Dai, X. Zhang, L. Zhang, T. Xu, A comparative study of the behavior of neural progenitor cells in extrusion-based in vitrohydrogel models, Biomed. Mater. 14 (2019), 065001.
[75] K. Schlett, A. Czirók, K. Tárnok, T. Vicsek, E. Madarász, Dynamics of cell aggregation during in vitro neurogenesis by immortalized neuroectodermal progenitors, J. Neurosci. Res. 60 (2000) 94–184.
[76] W. Kim, H. Lee, J. Lee, A. Atala, J.J. Yoo, S.J. Lee, G.H. Kim, Efficient myotube formation in 3D bioprinted tissue construct by biochemical and topographical cues, Biomaterials **230** (2020) 119632.
[77] R.K. Christensen, C. Halling Laier von, A. Kiziltay, S. Wilson, N.B. Larsen, 3D printed hydrogel multiassay platforms for robust generation of engineered contractile tissues, Biomacromolecules 21 (2020) 65–356.
[78] C.A. Schramm, R.S. Reiter, M. Solursh, Role for short-range interactions in the formation of cartilage and muscle masses in transfilter micromass cultures, Dev. Biol. 163 (1994) 79–467.
[79] T. Nakaji-Hirabayashi, K. Kato, H. Iwata, Hyaluronic acid hydrogel loaded with genetically-engineered brain-derived neurotrophic factor as a neural cell carrier, Biomaterials **30** (2009) 9–4581.
[80] Y. Kim, A.L. Larkin, R.M. Davis, P. Rajagopalan, The design of in vitroliver sinusoid mimics using chitosan–hyaluronic acid polyelectrolyte multilayers, Tissue Eng. **16** (2010) 41–2731.
[81] B. Svensson Holm A-C, T. Bengtsson, M. Grenegård, E.G. Lindström, Hyaluronic acid influence on platelet-induced airway smooth muscle cell proliferation, Exp. Cell Res. 318 (2012) 40–632.
[82] V. Desiderio, F. De Francesco, C. Schiraldi, A. De Rosa, A. La Gatta, F. Paino, R. d'Aquino, G.A. Ferraro, V. Tirino, G. Papaccio, Human Ng2+ adipose stem cells loaded in vivo on a new crosslinked hyaluronic acid-Lys scaffold fabricate a skeletal muscle tissue, J. Cell. Physiol. 228 (2013) 73–1762.
[83] P.A. Levett, F.P.W. Melchels, K. Schrobback, D.W. Hutmacher, J. Malda, T.J. Klein, A biomimetic extracellular matrix for cartilage tissue engineering centered on photocurable gelatin, hyaluronic acid and chondroitin sulfate, Acta Biomater. 10 (2014) 23–214.
[84] F. Sun, Y. Bu, Y. Chen, F. Yang, J. Yu, D. Wu, An injectable and instant self-healing medical adhesive for wound sealing, ACS Appl. Mater. Interfaces 12 (2020) 40–9132.
[85] Y. Li, Y.-Q. Chi, C.-H. Yu, Y. Xie, M.-Y. Xia, C.-L. Zhang, X. Han, Q. Peng, Drug-free and non-crosslinked chitosan scaffolds with efficient antibacterial activity against both Gram-negative and Gram-positive bacteria, Carbohydr. Polym. 241 (2020) 116386.